Lambda modes comparison for different approximations of the Neutron Transport Equation: Diffusion, SN and SP3

S. Morató[a], B. Kochunas[b], R. Miró[a], G. Verdú[a,*], E.W. Larsen[b], T. Downar[b]

[a] *Institute for Industrial, Radiophysical and Environmental Safety (ISIRYM) at the Universitat Politècnica de València, Spain*
[b] *Nuclear Engineering and Radiological Sciences (NERS) at the University of Michigan, Ann Arbor, Michigan*

Abstract

The methods presented in this paper solve the Simplified Spherical Harmonics approximation to the multidimensional neutron transport equation. 1D, 2D and 3D systems were modeled with Cartesian geometry using the finite difference method to discretize the spatial variables. The method is able to simulate any energy group discretization, including up-scattering terms. The Krylov Shur method was used to calculate the solution of the steady-state equation by solving a generalized eigenvalue problem. This methodology has the capability to calculate any number of eigenfunctions. A formulation review of the Simplified Spherical Harmonics is explained in this work, as well as, a study of the boundary conditions for different approaches of the finite difference method. The results calculated by this methodology are compared with the discrete ordinates and diffusion approximation methods, all of them, using the same spatial discretization in order to show the different accuracy of each method without influence of the method used for discretizing the spatial variable. The results show the validity of each method for different benchmark problems.

Keywords: Simplified Spherical Harmonics, SP3, Multigroup, Finite Difference Method, Multiple Eigenvalues, Boundary Conditions, lambda modes

1. Introduction

The diffusion equation is widely used in the analysis and design of nuclear reactors, which allows core calculations with reasonable computational time and accuracy. However, the diffusion approximation is valid only under 4 assumptions. The first is the assumption that the neutron current is proportional to the

*Corresponding author
Email address: `gverdu@iqn.upv.es` (G. Verdú)

neutron flux gradient. Second the medium is considered to have much less neutron absorption than scattering. Third, the angular dependence of the neutron flux is assumed to be linear. Fourth, the scattering is assumed isotropic.

For calculations in which the reactor core is characterized as an homogeneous, isotropic and diffusive medium, the diffusion approximation provides an accurate solution. Nevertheless, more detailed solutions, such as pin level calculations, are desired for improved accuracy. In cases where a control rod is considered, the highly absorbent material limits the applicability of the diffusion approximation. Therefore, more rigorous approximations for the neutron transport equation are required.

A more precise approach is to solve the neutron transport equation directly assuming a set of discrete angular directions. This method is called the discrete ordinates method (S_N). A review of this method was published by Bengt Carlson and Kaye Lathrop in 1964 [1]. At that time, the capabilities to solve complex problems with this methodology were limited, by the available computing power. Nowadays, the rapid progress of processors speed and the increase of the computer memory make possible the development of the S_N codes capable of simulating more complex and realistic problems. However, even with the current computers and improved algorithms, realistic problem can only be solved on the largest computers which require large amounts of memory and long calculations. Moreover, it is limited also by the finite number of digits in floating point calculations.

Another solution methodology uses the spherical harmonics (P_N) approximation to the neutron transport equation. This approximation is developed by using an expansion of the angular dependence of the flux into a set of spherical harmonic functions, which can be combined naturally with the Legendre functions to have an appropriate handle of the anisotropic scattering laws. Although, it is necessary to use an infinite order of the spherical harmonics to have an exact solution, only spherical harmonics up to order N are manageable for realistic analysis. The increase of the number of unknowns when multidimensional problems are considered have to be taken into account. One dimensional planar geometry use only $N+1$ equations for the P_N approximation. However, three-dimensional geometry needs $(N+1)^2$ number of equations making it relatively expensive to deal with. P_N equations can be reformulated as second order ones by defining even and odd parity fluxes: in such a way the number of unknowns remains significant and angular moments, as well as, spatial derivatives are present in the coupling.

For this reason the simplified spherical harmonics approximation (SP_N) appeared. This approximation was proposed by Gelbard in 1960 [2]. The idea is to replace the second derivatives in the one-dimensional planar geometry P_N equations with a general three-dimensional Laplacian operator [3]. In this way, the number of the required equations by SP_N approximation is fewer than P_N equations and the resulting system of equations can be solved by most of the standard diffusion solvers. Another advantage of the SP_N equations is that the problem which affects S_N equations known as the "ray effect" is not present when the SP_N equations are used.

However, the theoretical basis of the SP_N equations is continuously being discussed because its solution does not normally converge to the transport solution when $N \to \infty$.

The SP_3 and SP_5 are commonly used and their results present much better accuracy with respect to the diffusion approximation in most cases, giving results similar to transport solution.

In this work we show the discrepancies between three approximations to the resolution of the neutron transport equation. These approximations are diffusion, discrete ordinates method (S_N) and simplified spherical harmonics when $N = 3$ (SP_3). In order to perform a consistent comparison of the methods, all of them are formulated using finite difference method for the same spatial discretization.

The outline of the paper is as follows. Section 2 is devoted to define the formulation used to implement the SP_3 equations. Section 3 is focused on the method verification describing several benchmarks and showing their results. Finally, the last section, Section 4 summarize few comments and conclusions about the results.

2. Methods

This section shows a review of the simplified spherical harmonics (SP_N) equations, in particular when $N = 3$. Two different approaches of the finite difference method are explained and the way to implement the Marshak boundary conditions are studied in both cases.

Some different formulations to implement the simplified P_N equations have been published in several works. However, most of these do not include the details of the finite difference approximation of the boundary conditions. One of the most numerically and computationally efficient nomenclature is the one presented by Evans and Hamilton in [4]. However this work is based on the formulation developed by Brantley and Larsen [3] which presents more understandable nomenclature with better physical interpretation.

The SP_3 steady state equations can be classically written as [5]:

$$-\nabla(D_g\nabla[\phi_g^0+2\phi_g^2])+\Sigma_{r,g}[\phi_g^0+2\phi_g^2] = \frac{\chi_g}{K_{eff}}\sum_{g'}\nu\Sigma_{f,g'}\phi_{g'}^0+\sum_{g'\neq g}\Sigma_{s,g'\to g}\phi_{g'}^0+2\Sigma_{r,g}\phi_g^2, \tag{1}$$

$$-\frac{27}{35}\nabla(D_g\nabla\phi_g^2)+\Sigma_{t,g}\phi_g^2 = \frac{2}{5}\left\{\Sigma_{r,g}\phi_g^0-\left(\frac{\chi_g}{K_{eff}}\sum_{g'}\nu\Sigma_{f,g'}\phi_{g'}^0+\sum_{g'\neq g}\Sigma_{s,g'\to g}\phi_{g'}^0\right)\right\}. \tag{2}$$

In particular, for the one-dimensional case the eqs.1 and 2 can be expressed as:

$$\frac{\partial}{\partial x}(-D_g(x)\frac{\partial}{\partial x}\Phi_g(x)) + \Sigma_{r,g}(x)\Phi_g(x) =$$
$$\frac{\chi_g(x)}{K_{eff}}\sum_{g'}\nu\Sigma_{f,g'}(x)\phi^0_{g'}(x) + \sum_{g'\neq g}\Sigma_{s,g'\to g}(x)\phi^0_{g'}(x) + 2\Sigma_{r,g}(x)\phi^2_g(x), \quad (3)$$

$$\frac{27}{35}\frac{\partial}{\partial x}(-D_g(x)\frac{\partial}{\partial x}\phi^2_g(x)) + \Sigma_{t,g}(x)\phi^2_g(x) =$$
$$\frac{2}{5}\left\{\Sigma_{r,g}(x)\phi^0_g(x) - \left(\frac{\chi_g(x)}{K_{eff}}\sum_{g'}\nu\Sigma_{f,g'}(x)\phi^0_{g'}(x) + \sum_{g'\neq g}\Sigma_{s,g'\to g}(x)\phi^0_{g'}(x)\right)\right\}. \quad (4)$$

Where

$$\begin{aligned}
\Phi_g &= \phi^0_g + 2\phi^2_g \\
D_g &: \text{diffusion coefficient of group } g \\
\Sigma_{r,g} &: \text{removal cross section of group } g \text{ defined by} \\
&\quad \text{the sumation of absorption and out-scatter cross section.} \\
&\quad \Sigma_{r,g} = \Sigma_{a,g} + \sum_{g'\neq g}\Sigma_{s,g\to g'} = \Sigma_{t,g} - \Sigma_{s,g\to g} \\
\chi_g &: \text{fission spectrum of group } g \\
k_{eff} &: \text{multiplication factor} \\
\nu\Sigma_{f,g} &: \text{production cross section of group } g \\
\Sigma_{s,g'\to g} &: \text{scattering corss section from group } g' \text{ to } g \\
\Sigma_{t,g} &: \text{total cross section of group } g \\
\phi^m_g &: \text{neutron flux of the } m\text{-th order moment in group } g
\end{aligned}$$

Two finite difference methods are derived in the following sections. The first considers the flux in the center of each subdivision or cell. The second one, uses a edge-centered approach defining the unknowns on the boundary. The cell centered approach have more physical sense than the edge-centered approach, because it considers the cross sections in the middle of the cell while the edge-centered approach needs to use an average cross section. However, the authors find interesting to compare both approaches.

2.1. Method 1: Cell-centered Finite Difference Method

The coupled SP_3 equations discretized using cell-centered finite difference method are:

$$
\begin{aligned}
&-\widetilde{D}^0_{i-1,g}\Phi_{i-1,g} + [\widetilde{D}^0_{i-1,g} + \widetilde{D}^0_{i,g} + \Sigma_{r,i,g}h_i]\Phi_{i,g} - \widetilde{D}^0_{i,g}\Phi_{i+1,g} = \\
&\qquad \frac{\chi_{i,g}}{K_{eff}} \sum_{g'} \nu\Sigma_{f,i,g'} h_i \phi^0_{i,g'} + \sum_{g' \neq g} \Sigma_{s,i,g' \to g} h_i \phi^0_{i,g'} + 2\Sigma_{r,i,g} h_i \phi^2_{i,g},
\end{aligned} \tag{5}
$$

$$
\begin{aligned}
&-\widetilde{D}^2_{i-1,g}\phi^2_{i-1,g} + [\widetilde{D}^2_{i-1,g} + \widetilde{D}^2_{i,g} + \Sigma_{t,i,g}h_i]\phi^2_{i,g} - \widetilde{D}^2_{i,g}\phi^2_{i+1,g} = \\
&\quad \frac{2}{5}\Sigma_{r,i,g} h_i \phi^0_{i,g} - \frac{2}{5}\frac{\chi_{i,g}}{K_{eff}} \sum_{g'} \nu\Sigma_{f,i,g'} h_i \phi^0_{i,g'} - \frac{2}{5} \sum_{g' \neq g} \Sigma_{s,i,g' \to g}(x) h_i \phi^0_{i,g'},
\end{aligned} \tag{6}
$$

where:

$$
\widetilde{D}^m_{i,g} = \frac{2D^m_{i,g}D^m_{i+1,g}}{D^m_{i,g}h_{i+1} + D^m_{i+1,g}h_i}, \tag{7}
$$

$$
\widetilde{D}^m_{i-1,g} = \frac{2D^m_{i-1,g}D^m_{i,g}}{D^m_{i-1,g}h_i + D^m_{i,g}h_{i-1}}, \tag{8}
$$

$$
\begin{aligned}
m =& 0, 2, \\
\Phi_{i,g} =& \phi^0_{i,g} + 2\phi^2_{i,g}, \\
D^0_{i,g} =& D_{i,g} = \frac{1}{3\Sigma_{t,i,g}}, \\
D^2_{i,g} =& \frac{27}{35} D_{i,g}.
\end{aligned}
$$

The derivation of these equations is shown in Appendix A.

2.2. SP_3 boundary conditions applied to the cell-centered Scheme

The SP_3 vacuum boundary conditions for these equations are given by ([6], [3], [4]). The Marshak-like boundary conditions for vacuum can be expressed as:

$$
D^0_{i,g} \overrightarrow{n} \cdot \nabla \Phi_{i,g} + \frac{1}{2}\phi^0_{i,g} + \frac{5}{8}\phi^2_{i,g} = 0, \tag{9}
$$

$$
D^2_{i,g} \overrightarrow{n} \cdot \nabla \phi^2_{i,g} - \frac{3}{40}\phi^0_{i,g} + \frac{3}{8}\phi^2_{i,g} = 0, \tag{10}
$$

Where:

$$
\begin{aligned}
\Phi_{i,g} =& \phi^0_{i,g} + 2\phi^2_{i,g}, \\
D^0_{i,g} =& D_{i,g} = \frac{1}{3\Sigma_{t,i,g}}, \\
D^2_{i,g} =& \frac{27}{35} D_{i,g} = \frac{9}{35\Sigma_{t,i,g}}.
\end{aligned}
$$

Marshak boundary conditions are easy to implement in a finite difference edge-centered approach or finite element method where some unknowns are the points considered at the boundary interface. However, considering the finite difference cell-centered approach it is necessary to relate the flux in the middle of the cell close to the boundary surface with the flux considered at the boundary interface. This is not straightforward task and three different approaches are considered in the next section.

The SP_3 reflective boundary conditions are more straightforward. These can be obtained:

$$\nabla \Phi_{i,g} = 0, \tag{11}$$

$$\nabla \phi^2_{i,g} = 0. \tag{12}$$

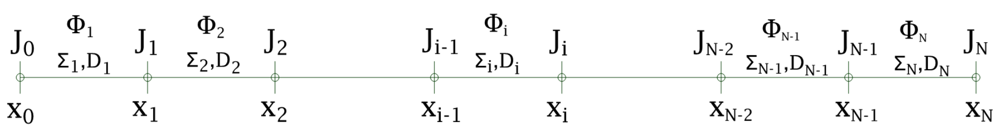

Figure 1: Discretization Scheme

2.2.1. First vacuum B.C. approach: $\phi^0_{x_0,g} = \phi^0_{1,g}$ and $\phi^2_{x_0,g} = \phi^2_{1,g}$

In this case we assume that the flux on the left boundary is the same as the flux in the middle of the first cell. Then, the eqs.13 and 14 can be introduced into the balance eqs.A.9 and A.24. This approach is not recommended. Depending on the problem, the solution using this approach could be more different with respect to a finely meshed transport. One simple solution to obtain good results in these cases with this approach is to use a finer mesh close to the boundary.

$$J^0_{x_0,g} = -\frac{1}{2}\phi^0_{1,g} - \frac{5}{8}\phi^2_{1,g}, \tag{13}$$

$$J^2_{x_0,g} = \frac{3}{40}\phi^0_{1,g} - \frac{3}{8}\phi^2_{1,g}. \tag{14}$$

2.2.2. Second vacuum B.C. approach

This approach provides better results than the previous one. Here the boundary conditions are defined in a similar way to the diffusion equations but only for the first moment $\phi^0_{x_0,g}$. We can obtain the P_1 equation starting from SP_3 equations by removing the second SP_3 equation for the 2nd moment (eq.2) and by removing ϕ^2_g inside the first SP_3 equation for the zero moment (eq.1). We can do the same with the boundary conditions. So, the balance equation is:

$$-D_g \nabla^2 \phi^0_g + \Sigma_{r,g}\phi^0_g = \frac{\chi_g}{K_{eff}} \sum_{g'} \nu\Sigma_{f,g'}\phi^0_{g'} + \sum_{g' \neq g} \Sigma_{s,g' \to g}\phi^0_{g'}, \tag{15}$$

The left boundary condition equation used in the diffusion equation where $\alpha = 1/2$ for the vacuum condition is:

$$J_{x_0,g} = -\alpha_L \cdot \phi_{x_0,g} = -D_1 \frac{\phi_{1,g} - \phi_{x_0,g}}{h_1/2}, \tag{16}$$

$$J_{x_0,g} = -2\frac{(D_{1,g}/h_1)(\alpha_L/2)}{[(D_{1,g}/h_1) + (\alpha_L/2)]}\phi_{1,g} = -\widetilde{D}_{0,g}\phi_{1,g}, \tag{17}$$

with $\alpha_L = 1/2$ we have the Marshak vacuum boundary condition for P_1 (Diffusion) equation:

$$J_{x_0,g} = -\frac{1}{2}\frac{(D_{1,g}/h_1)}{[(D_{1,g}/h_1) + (1/4)]}\phi_{1,g}, \tag{18}$$

Taking this into account, we should do something similar for the SP_3 equations, but in this case the solution for the boundary condition is not so straighforward, due to the second moment flux. We can see that in the next equation which corresponds to the eq.16, but for the first SP_3 equation:

$$J^0_{x_0,g} = -\alpha_L \cdot \phi^0_{x_0,g} - \beta_L \cdot \phi^{2,L}_{0,g} = -D_{1,g}\frac{\phi^0_{1,g} + 2\phi^2_{1,g} - \phi^0_{x_0,g} - 2\phi^2_{x_0,g}}{h_1/2}, \tag{19}$$

For obtaining a more simple solution we can approximate the SP_3 boundary conditions by adding the term of the eq.18 defined for P_1 equation into the SP_3 first moment boundary condition equation .

$$J^0_{x_0,g} = -\frac{1}{2}\frac{(D_{1,g}/h_1)}{[(D_{1,g}/h_1) + (1/4)]}\phi^0_{1,g} - \frac{5}{8}\phi^2_{1,g}, \tag{20}$$

$$J^2_{x_0,g} = \frac{3}{40}\phi^0_{1,g} - \frac{3}{8}\phi^2_{1,g}. \tag{21}$$

Although this is not the exact solution, the numerical results are significantly better than those obtained with the previous simplification.

2.2.3. Third approach: Exact vacuum B.C. for SP3

In this section the exact boundary conditions for SP_3 using the cell-centered finite difference are defined. Starting from the eqs.9 and 10 and the Fick's law, the left boundary equations are:

$$J^0_{x_0,g} = -\frac{1}{2}\phi^0_{x_0,g} - \frac{5}{8}\phi^2_{x_0,g}, \tag{22}$$

$$J^2_{x_0,g} = \frac{3}{40}\phi^0_{x_0,g} - \frac{3}{8}\phi^2_{x_0,g}, \tag{23}$$

In order to have the same number of unknowns and equations we need to define eqs.22 and 23 in terms of $\phi^0_{1,g}$ and $\phi^2_{1,g}$. To that, we define:

$$J^0_{x_0,g} = -\frac{D^0_{1,g}}{h_1/2}[\Phi_{1,g} - \Phi_{x_0,g}] = -\frac{D^0_{1,g}}{h_1/2}[(\phi^0_{1,g} + 2\phi^2_{1,g}) - (\phi^0_{x_0,g} + 2\phi^2_{x_0,g})], \tag{24}$$

$$J^2_{x_0,g} = -\frac{27}{35}\cdot\frac{D^0_{1,g}}{h_1/2}[\phi^2_{1,g} - \phi^2_{x_0,g}], \tag{25}$$

Eqs. 22 and 23 will now be solved for $\phi^0_{x_0,g}$ and $\phi^2_{x_0,g}$ in terms of $J^0_{x_0,g}$ and $J^2_{x_0,g}$. Multiplying eq.23 by 20/3 :

$$\frac{20}{3}J^2_{x_0,g} - \frac{1}{2}\phi^0_{x_0,g} + \frac{5}{2}\phi^2_{x_0,g} = 0,$$

Adding this to eq.22 gives:

$$J^0_{x_0,g} + \frac{20}{3}J^2_{x_0,g} + \left[\frac{5}{8} + \frac{5}{2}\right]\phi^2_{x_0,g} = 0,$$

So,

$$\phi^2_{x_0,g} = -\frac{8}{25}J^0_{x_0,g} - \frac{32}{15}J^2_{x_0,g}, \tag{26}$$

Introducing this result into eq.22, we get

$$\phi^0_{x_0,g} = -\frac{8}{5}J^0_{x_0,g} + \frac{8}{3}J^2_{x_0,g}, \tag{27}$$

Now, we introduce eqs.26 and 27 into eqs.24 and 25 to get:

$$J^0_{x_0,g} = -\frac{2D^0_{1,g}}{ah_1}\left[\phi^0_{1,g} + 2\phi^2_{1,g} + \frac{8}{5}J^2_{x_0,g}\right], \tag{28}$$

$$J^2_{x_0,g} = -\frac{27}{35}\cdot\frac{2D^0_{1,g}}{bh_1}\left[\phi^2_{1,g} + \frac{8}{25}J^0_{x_0,g}\right], \tag{29}$$

where:

$$a = \left[1 + \frac{112}{25} \cdot \frac{D^0_{1,g}}{h_1}\right], \qquad b = \left[1 + \frac{27}{35} \cdot \frac{32}{15} \cdot \frac{2D^0_{1,g}}{h_1}\right],$$

Introducing eq.29 into eq.28 we get:

$$J^0_{x_0,g} = -\frac{2D^0_{1,g}}{ach_1}\phi^0_{1,g} - \frac{4D^0_{1,g}}{ach_1}(1 - \frac{216}{175} \cdot \frac{D^0_{1,g}}{bh_1})\phi^2_{1,g}, \tag{30}$$

where:

$$c = \left[1 - \frac{2D^0_{1,g}}{ah_1}\left(\frac{1728}{4375} \cdot \frac{2D^0_{1,g}}{bh_1}\right)\right],$$

Introducing eq.30 into eq.29 we get:

$$J^2_{x_0,g} = -\frac{27}{35} \cdot \frac{2D^0_{1,g}e}{bh_1}\phi^0_{1,g} - \frac{27}{35} \cdot \frac{2D^0_{1,g}d}{bh_1}\phi^2_{1,g}, \tag{31}$$

where:

$$d = \left[1 - \frac{8}{25} \cdot \frac{4D^0_{1,g}}{ach_1}\left(1 - \frac{216}{175} \cdot \frac{D^0_{1,g}}{bh_1}\right)\right], \qquad e = \left[-\frac{8}{25} \cdot \frac{D^0_{1,g}}{ach_1}\right].$$

Eqs.30 and 31 can be introduced into the balance eqs.A.9 and A.24 to apply vacuum boundary condition.

2.2.4. Reflective and Zero flux boundary condition for SP_3

Reflective and zero flux boundary conditions are more straightforward. To implement reflective boundary condition just we set:

$$J^0_{x_0,g} = 0, \qquad \text{and} \qquad J^2_{x_0,g} = 0,$$

Zero flux boundary condition means that $\phi^0_{x_0,g} = 0$ and $\phi^2_{x_0,g} = 0$ into eqs.24 and 25. So, just we set:

$$J^0_{x_0,g} = -\frac{D^0_{1,g}}{h_1/2}\left(\phi^0_{1,g} + 2\phi^2_{1,g}\right), \qquad \text{and} \qquad J^2_{x_0,g} = -\frac{27}{35} \cdot \frac{D^0_{1,g}}{h_1/2}\phi^2_{1,g}.$$

2.3. Method 2: Edge-centered Finite Difference Method

The coupled SP_3 equations discretized using edge-centered finite difference method are:

$$\left[\frac{D^0_{g,i+1}}{h_{i+1}} + \frac{D^0_{g,i}}{h_i} + \overline{\Sigma}_{r,g,i}\right]\Phi_{g,i} - \frac{D^0_{g,i+1}}{h_{i+1}}\Phi_{g,i+1} - \frac{D^0_{g,i}}{h_i}\Phi_{g,i-1} - 2\overline{\Sigma}_{r,g,i}\phi^2_{g,i} = \frac{\chi_{g,i}}{K_{eff}}\sum_{g'}\overline{\nu\Sigma}_{f,g',i}\phi^0_{g',i} + \sum_{g'\neq g}\overline{\Sigma}_{s,g'\to g,i}\phi^0_{g',i}, \quad (32)$$

$$\left[\frac{D^2_{g,i+1}}{h_{i+1}} + \frac{D^2_{g,i}}{h_i} + \overline{\Sigma}_{t,g,i}\right]\phi^2_{g,i} - \frac{D^2_{g,i+1}}{h_{i+1}}\phi^2_{g,i+1} - \frac{D^2_{g,i}}{h_i}\phi^2_{g,i-1} - \frac{2}{5}\overline{\Sigma}_{r,g,i}\phi^0_{g,i} = -\frac{2}{5}\frac{\chi_{g,i}}{K_{eff}}\sum_{g'}\overline{\nu\Sigma}_{f,g',i}\phi^0_{g',i} - \frac{2}{5}\sum_{g'\neq g}\overline{\Sigma}_{s,g'\to g,i}\phi^0_{g',i}. \quad (33)$$

The derivation of these equations can be found in Appendix B.

2.3.1. Left vacuum boundary condition ($i = 0$)

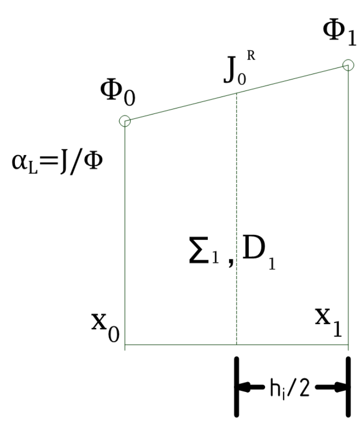

Figure 2: Left boundary conditions edge-centered scheme

Considering the Fick's Law and $\overrightarrow{n} = -1$ on the left boundary, we can write eq.9 and 10 as:

$$J^0_{g,0} = -\frac{1}{2}\phi^0_{g,0} - \frac{5}{8}\phi^2_{g,0}, \quad (34)$$

$$J^2_{g,0} = \frac{3}{40}\phi^0_{g,0} - \frac{3}{8}\phi^2_{g,0}, \tag{35}$$

Introducing eqs.34 and B.8 into the balance equation eq.B.6 we have the eq.36 when $i = 0$:

$$\left[\frac{D^0_{g,i+1}}{h_{i+1}} + \overline{\Sigma}_{r,g,i}\right]\Phi_{g,i} + \left(\frac{1}{2}\phi^0_{g,i} + \frac{5}{8}\phi^2_{g,i}\right) - \frac{D^0_{g,i+1}}{h_{i+1}}\Phi_{g,i+1} - 2\overline{\Sigma}_{r,g,i}\phi^2_{g,i} = \frac{\chi_{g,i}}{K_{eff}}\sum_{g'}\overline{\nu\Sigma}_{f,g',i}\phi^0_{g',i} + \sum_{g'\neq g}\overline{\Sigma}_{s,g'\to g,i}\phi^0_{g',i}, \tag{36}$$

And introducing eq.35 into the balance equation for the second moment we have eq.37 when $i = 0$:

$$\left[\frac{D^2_{g,i+1}}{h_{i+1}} + \overline{\Sigma}_{t,g,i}\right]\phi^2_{g,i} + \left(\frac{-3}{40}\phi^0_{g,i} + \frac{3}{8}\phi^2_{g,i}\right) - \frac{D^2_{g,i+1}}{h_{i+1}}\phi^2_{g,i+1} - \frac{2}{5}\overline{\Sigma}_{r,g,i}\phi^0_{g,i} = -\frac{2}{5}\frac{\chi_{g,i}}{K_{eff}}\sum_{g'}\overline{\nu\Sigma}_{f,g',i}\phi^0_{g',i} - \frac{2}{5}\sum_{g'\neq g}\overline{\Sigma}_{s,g'\to g,i,}\phi^0_{g',i}. \tag{37}$$

2.3.2. Right vacuum boundary condition ($i = N$)

Using the same procedure than left boundary but with $\overrightarrow{n} = 1$:

$$J^0_{g,N} = \frac{1}{2}\phi^0_{g,N} + \frac{5}{8}\phi^2_{g,N}, \tag{38}$$

$$J^2_{g,N} = -\frac{3}{40}\phi^0_{g,N} + \frac{3}{8}\phi^2_{g,N}, \tag{39}$$

Introducing eq.38 into the balance eq.B.6 we have the eq.40 when $i = N$:

$$\left[\frac{D^0_{g,i}}{h_i} + \overline{\Sigma}_{r,g,i}\right]\Phi_{g,i} + \left(\frac{1}{2}\phi^0_{g,N} + \frac{5}{8}\phi^2_{g,N}\right) - \frac{D^0_{g,i}}{h_i}\Phi_{g,i-1} - 2\overline{\Sigma}_{r,g,i}\phi^2_{g,i} = \frac{\chi_{g,i}}{K_{eff}}\sum_{g'}\overline{\nu\Sigma}_{f,g',i}\phi^0_{g',i} + \sum_{g'\neq g}\overline{\Sigma}_{s,g'\to g,i}\phi^0_{g',i}, \tag{40}$$

And introducing eq.39 into the balance equation for the second moment we have eq.41 when $i = N$:

$$\left[\frac{D^2_{g,i}}{h_i} + \overline{\Sigma}_{t,g,i}\right]\phi^2_{g,i} + \left(\frac{-3}{40}\phi^0_{g,N} + \frac{3}{8}\phi^2_{g,N}\right) - \frac{D^2_{g,i}}{h_i}\phi^2_{g,i-1} - \frac{2}{5}\overline{\Sigma}_{r,g,i}\phi^0_{g,i} = \\ -\frac{2}{5}\frac{\chi_{g,i}}{K_{eff}}\sum_{g'}\overline{\nu\Sigma}_{f,g',i}\phi^0_{g',i} - \frac{2}{5}\sum_{g'\neq g}\overline{\Sigma}_{s,g'\to g,i}\phi^0_{g',i}. \quad (41)$$

To derive the multidimensional formulations one can derive it from the one dimensional formulations stated in this section. These formulations can be easily extrapolated to two-dimensional and three-dimensional problems. Multidimensional formulations have not been presented in this work for brevity. The numerical results in section 3 include multidimensional results.

The authors want to highlight that the presentation of the discretized vacuum boundary conditions have not been presented in other works. Prior to Brantley the correct expression might not have been known. Given the complexity of the vacuum boundary conditions it is possible early methods were using approximate vacuum boundary conditions.

2.4. Krylov method

The power iteration method is commonly used for solving the eigenvalue problem generated from the different approximations of the neutron transport equation. Nevertheless, the dominance ratio that determine the degree of convergence is normally close to 1 in the nuclear field, reducing the convergence speed of the method. For this reason, the use of Krylov methods suppose an advantage to solve those problems which have a high dominance ratio, allowing to achieve the solution faster than the power iteration method as can be seen in [7] among others. Furthermore, another important advantage of the Krylov methods is the possibility of calculating several eigenvalues, not only the fundamental mode, but also the subcritical ones. In this regard, the nuclear field is using more and more this kind of methods, particularly the Krylov-Schur is one of the most used recently, [8].

The methods developed in this work use the Krylov-Schur algorithm embedded into the SLEPc library to solve the eigenvalue problem. This is a very commonly used software library specially intended for solving eigenproblems of large and sparse matrices [9]. SLEPc needs PETSc to be completely functional and to be able of calculating the solution of eigenvalue problems. PETSc includes matrix operations as well as the solution of linear systems [10]. Several iterative methods to solve the system of linear equations were tested, but finally the method implemented was the generalized minimal residual method (GMRES) using as a preconditioner an incomplete LU factorization.

3. Numerical Results

The numerical methods explained in the previous section have been implemented in a FORTRAN code called *SHE3NA* (simplified Spherical Harmonics Equations sp3 Neutron Aproximation). This code implements the SP_3 equations explained above, as well as a Diffusion code (SP_1). Furthermore, *SHE3NA* has been compared with other neutron transport approximations exposed and validated in the previous work [11] where S_N method was introduced. Different neutron transport codes are used as a reference to compare the results of the developed SP_3 code. Next sections make use of some standard codes as reference values, such as the Discrete Ordinates based method code DANTSYS, as well as FEMFUSSION, a finite element SP_3 method developed by A. Vidal-Ferrndiz [12]. Another code based on the discrete ordinates method mentioned before is used as a reference, which was validated in [11]. Furthermore, analytical solutions from [13] are compared with the results calculated by the algorithms implemented in this work.

This section shows several numerical results for 1D, 2D and 3D benchmark problems, some of them described in the previous work [11]. The results show eigenvalues comparison for the fundamental and subcritical modes between the considered neutron transport approximations, as well as neutron flux comparison.

3.1. Homogeneous slab reactor

This problem considers a one-group homogeneous slab 2 cm thick with $\Sigma_t = 1.0\ cm^{-1}$, $\nu\Sigma_f = 0.25\ cm^{-1}$ and $\Sigma_s = 0.9\ cm^{-1}$. This problem can be found in [14] solved by P_1, P_3, P_5 and with transport code ONEDANT. The multiplication factors are shown in tables 1 and 3 for P_1, P_3, whose values are analytic solutions [14],and for the FDM SP_3 and diffusion code developed. The solution for the FDM SP_3 and diffusion code is calculated using a mesh of 2048 cells.

Table 1: First 4 eigenvalues - homogeneous slab reactor.*($Dif.^C$ is the SP_1 code using cell-centered sheme.) ($Dif.^E$ is the SP_1 code using edge-centered Scheme.)*

Eig.	P_1 Analytic Sol.	FDM $Dif.^C$	FDM $Dif.^E$
1st	0.587489	0.587489	0.587489
2nd	0.149135	0.149135	0.149135
3rd	0.058380	0.058380	0.058380
4th	0.029602	0.029602	0.029602

The compared scalar flux can be seen at fig.3. It was compared with a neutron transport code using S_{16} and with another SP_3 code called FEMFFUSION which uses the finite element method to discretize the spatial variables [12]. The flux curves calculated with FDM SP_3^c and FDM SP_3^E are overlapping in fig.3.

It can be seen that the eigenvalues calculated by the diffusion code and the SP_3 code differ 0 pcm with respect to the analytical solutions. Regarding to

Table 2: First 4 eigenvalues - homogeneous slab reactor. *(SP_3^C is the SP_3 code using cell-centered scheme.) (SP_3^E is the SP_3 code edge-centered scheme.)*

Eig.	SP_3 Analytical Sol.	FDM SP_3^C	FDM SP_3^E	FDM S_{16}
1st	0.652956	0.652956	0.652956	0.659847
2nd	0.207745	0.207745	0.207745	0.225817
3rd	0.096091	0.096092	0.096091	0.119940
4th	0.053122	0.053122	0.053122	0.075487

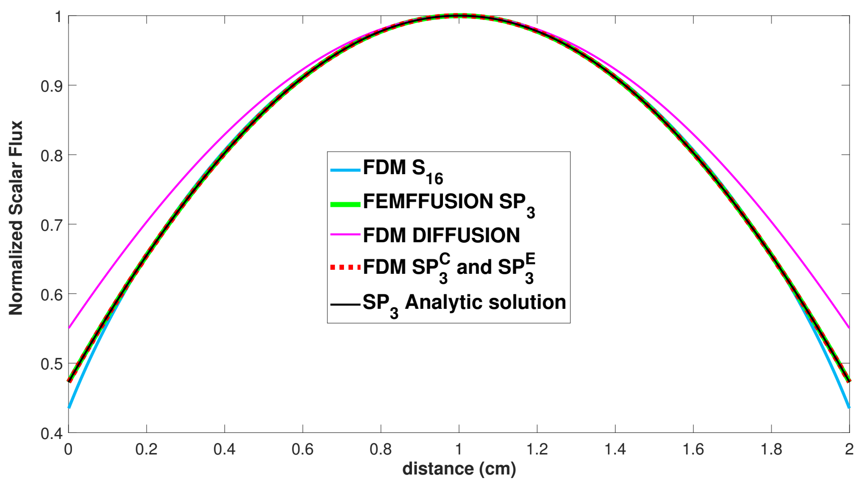

Figure 3: Normalized Scalar Flux for Homogeneous 1D reactor

the flux comparison, fig.3 shows that the SP_3 approximation is more accurate than the diffusion solution, and it is not as accurate as the transport solution S_{16} as expected.

3.1.1. Boundary conditions comparison

This section shows the differences between the three vacuum boundary approaches explained in sections 2.2.1, 2.2.2 and 2.2.3, for the one-dimensional homogeneous problem.

As can be seen in table 3, the exact solution is only achieved with the third vacuum boundary condition approach (BC3). The second approach (BC2) differs 1 pcm from the exact solution for the fundamental mode, while the first approach (BC1) differs 10 pcm for the fundamental mode. All the results were calculated with the same discretization. Better results can be obtained using first and second approaches if the number of points of the discretization is increased.

These results would indicate, that in 1D evaluations of numerical implementations, it would be difficult to ascertain that the incorrect boundary conditions

Table 3: First 4 eigenvalues - homogeneous slab reactor. *(SP_3^{C*} is the SP_3 code using cell-centered scheme and BC refers to each boundary condition approach.)*

Eig.	SP_3 Analytical Sol.	FDM SP_3^C BC3	FDM SP_3^C BC2	FDM $SP_3^C BC1$
1st	0.652956	0.652956	0.652890	0.652493
2nd	0.207745	0.207745	0.207702	0.207621
3rd	0.096091	0.096092	0.096074	0.096052
4th	0.053122	0.053122	0.053115	0.053107

are truly incorrect without careful intensive evaluation. The differences observed in the eigenvalues could easily be assumed to be the result of a spatial discretization error. This is further observed in fig.4, where again, the solutions with the inexact boundary conditions are very close to the correct result.

This effect becomes more pronounced in multidimensional problems which is discussed later in section 3.6.

Fig.4 shows the normalized scalar flux calculated with the three different boundary condition approaches. In this case, the difference between the normalized scalar fluxes calculated with the three approaches can be considered negligible.

3.2. Heterogeneous slab test problem

This problem is configured by seven slab regions of fuel and reflector [14]. Table 4 shows the cross section of the each material considering one-energy group. A scheme of the problem is shown in fig.5. Vacuum conditions are considered for left and right boundaries. The number of mesh cells for each region are 500. The four largest eigenvalues are shown in table 5. The reference values from [14] were compared with the calculated results. One can see that the values obtained with the developed code SP_3 are in agreement with the reference values P_3. The scalar flux is compared in figs.6-9 for the four modes. The FDM SP_3 scalar flux is also compared with S_{96} and the FEMFFUSION code. The S_{96} codes are DANTSYS and the FDM S_{96} developed by the author in [11]. The accuracy of the SP_3 equations is better than the diffusion results and similar to the S_{96} values.

Table 4: Cross-Sections for heterogeneous slab problem

	$\nu\Sigma_f(cm^{-1})$	$\Sigma_s(cm^{-1})$	$\Sigma_t(cm^{-1})$
Fuel (U-235)	0.178	0.334	0.416667
Reflector	0.0	0.334	0.370370

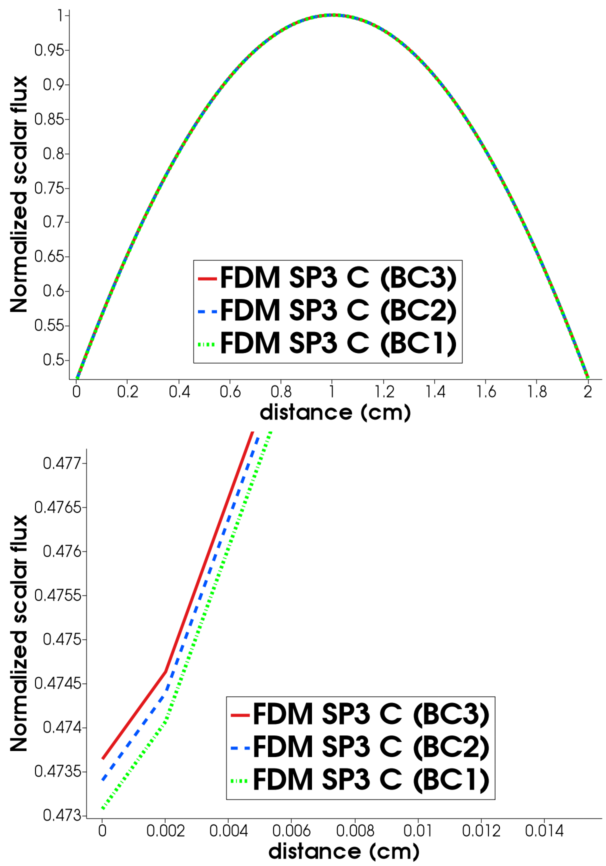

Figure 4: Normalized Scalar Flux for Homogeneous 1D reactor and detail of the boundary

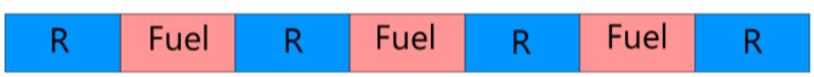

Figure 5: Scheme ot the 7 region problem

Table 5: Heterogeneous slab problem eigenvalues *(SP_3^C is the SP3 code using cell-centered scheme, SP_3^E is the SP3 code using edge-centered scheme.)*

Eig.	P_3	PARTISN S_{96}	FDM S_{96}	FDM SP_3^C	FDM SP_3^E	FDM $Diff.^C$
1st	1.148740	1.162413	1.162228	1.148745	1.148744	1.113872
2nd	0.735037		0.752258	0.735037	0.735037	0.658651
3rd	0.527647		0.547565	0.527647	0.527646	0.423945
4th	-		0.210955	0.165351	0.165350	0.109256

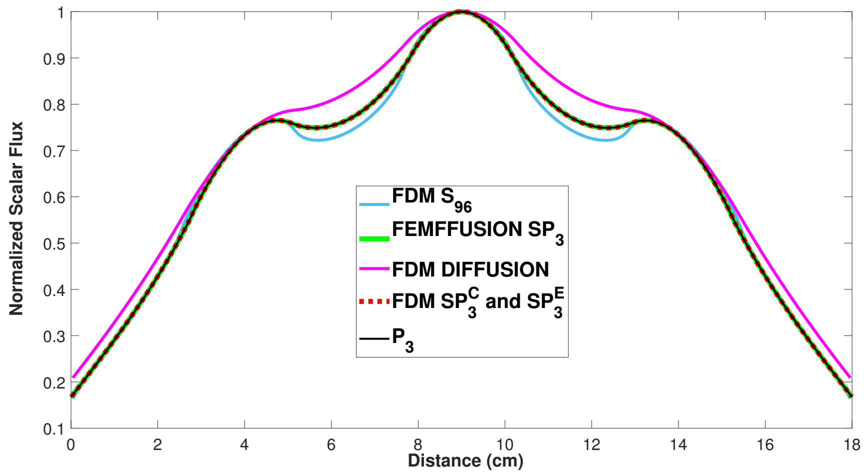

Figure 6: Normalized Scalar Flux for heterogeneous slab problem: mode 1

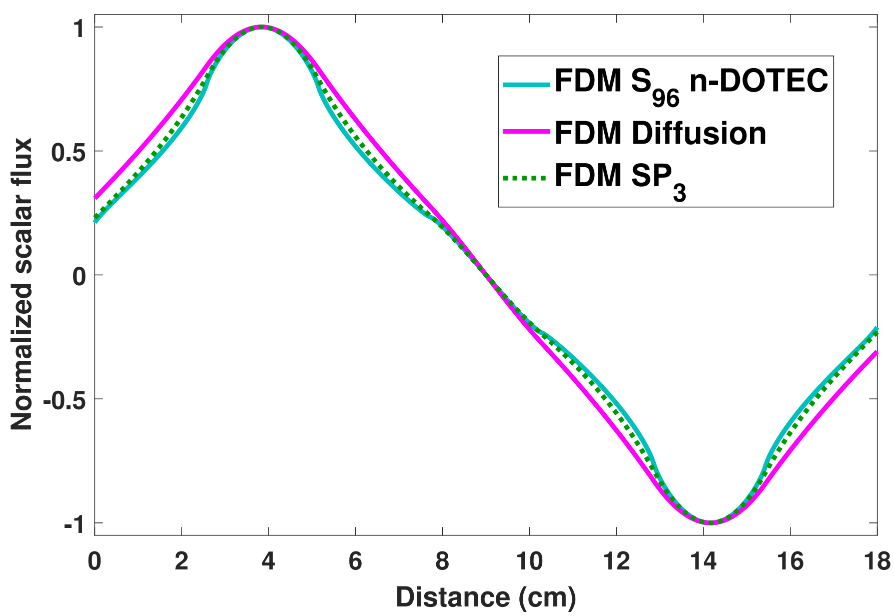

Figure 7: Normalized Scalar Flux for heterogeneous slab problem: mode 2

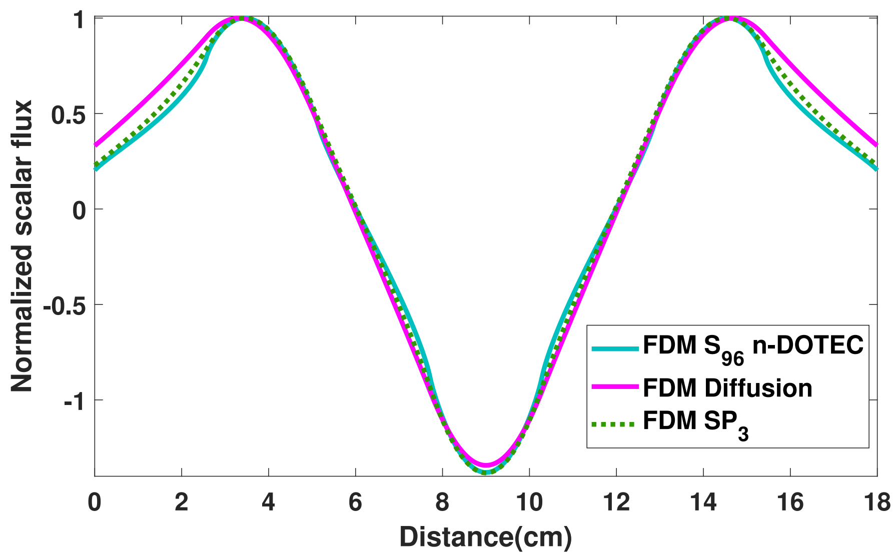

Figure 8: Normalized Scalar Flux for heterogeneous slab problem: mode 3

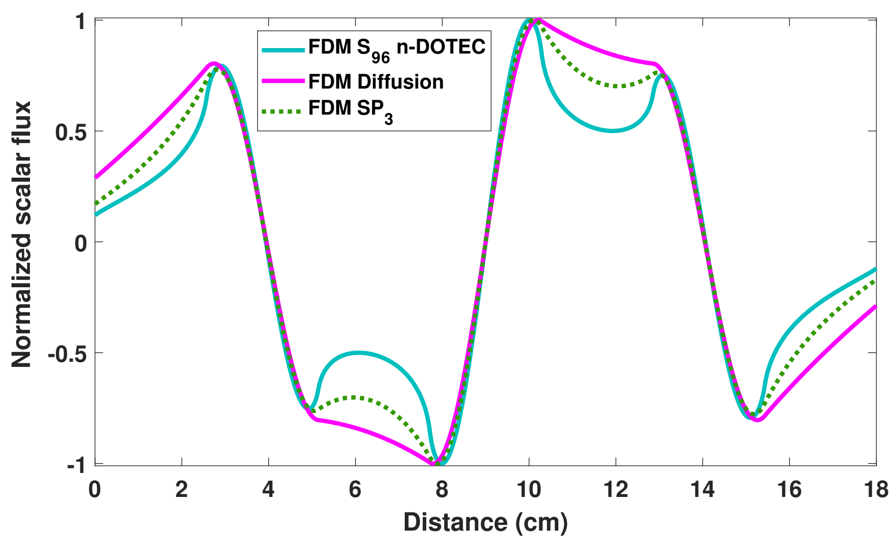

Figure 9: Normalized Scalar Flux for heterogeneous slab problem: mode 4

3.3. MOX benchmark problem

The MOX benchmark problem corresponds to a modification of the MOX problem, defined in [13] which was adapted from [3]. Two types of fuel (MOX/UO_2) configuration of 7×7 fuel assemblies composes the complete core as seen in fig.10. There is a reflector material surrounding the core and each assembly measures 21.42 cm ×21.42 cm. Three different materials with two-energy cross section describe the problem, as shown in table 6. Vacuum is considered for all boundary conditions.

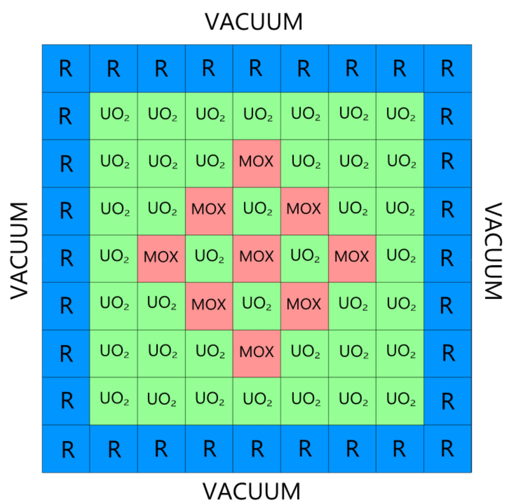

Figure 10: MOX benchmark problem geometry

Four dominant eigenvalues were compared taking as reference the eigenvalues calculated by Spherical Harmonics Nodal Collocation (SHNC) method in [13]. The comparison is shown in table 7. Both, SP_3 and diffusion calculations were generated with a discretization of 50 cells in x and y axis for each assembly as well as the calculation by using S_8 method. In figs.11 and 12, the neutron scalar flux is shown for the first, second, third and fourth modes. In this case, it can be appreciated that eigenvalues calculated with the SP_3 using the cell-centered scheme shows better accuracy than edge-centered one and diffusion approximation. However, analogous improvement cannot be seen in the flux distribution. This could be because the problem is highly diffusive. Moreover, the authors want to point out that cross-sections of both fuels are very similar. With regards to the eigenflux comparison between SP_3 and S_8, it is important to highlight that the eigenfluxes corresponding to 2nd and 3rd mode, which are degenerate due to the fact that they have the same eigenvalue, do not have exactly the same distribution. This is a normal condition considering symmetric problems since both eigenfluxes are a linear combination of the solution, and any linear combination could be a solution for this kind of problems although, physically it does not make sense. However, it can be seen that regarding the 4th eigenflux, the shape is similar.

Table 6: Cross-sections of the MOX benchmark problem. Thermal group is g=2.

Material	Group	Σ_t	$\nu\Sigma_f$	$\Sigma_{s,1\rightarrow g}$	$\Sigma_{s,2\rightarrow g}$	χ_g
MOX fuel	1	0.550	0.0075	0.520	-	1.000
	2	1.060	0.450	0.015	0.760	0.000
UO_2 fuel	1	0.570	0.005	0.540	-	1.000
	2	1.100	0.125	0.020	1.000	0.000
Reflector	1	0.611	0.000	0.560	-	0.000
	2	2.340	0.000	0.050	2.300	0.000

Table 7: First 4 modes - MOX problem. **Spherical Harmonics Nodal Collocation (SHNC).*

Eigenv.	SHNC*	FDM SP_3^C	FDM $Dif.^C$	FDM SP_3^E	FDM $Dif.^E$	FDM S_8
k_{eff}	0.9925	0.992505	0.992876	0.992819	0.993133	0.992608
2nd eigen.	0.9665	0.966475	0.966665	0.966721	0.966868	0.966544
3rd eigen.	0.9665	0.966475	0.966665	0.966721	0.966868	0.966544
4th eigen.	0.9399	0.939879	0.939807	0.940019	0.939926	0.939900

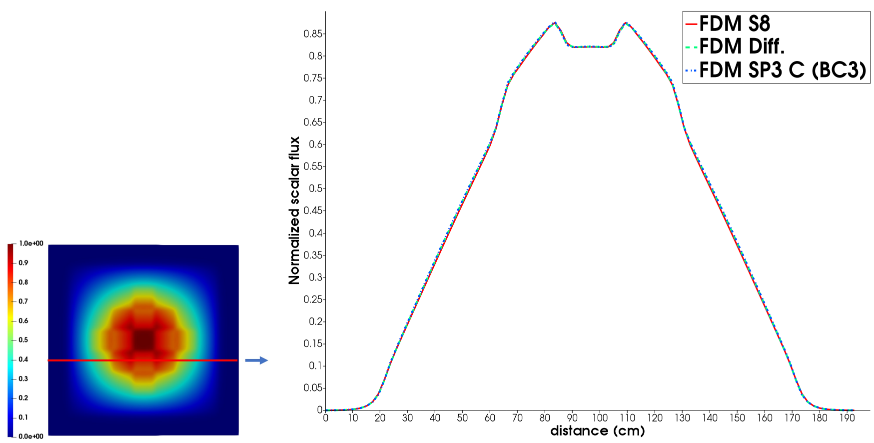

Figure 11: MOX: First energy group scalar flux distribution for 1st eigenvalue

3.4. BWR cell benchmark problem

The following case corresponds to an homogeneous BWR cell [15, 16]. The consideration of the upscattering in this case is one of the reasons why it was selected for this work. The problem is composed of water moderator surrounding a central homogenized fuel region as it can be seen in fig.13. Two materials form the problem and their cross-sections with two-energy groups are presented in table 8. Reflective boundary conditions are considered. The reference multiplication factor calculated with DANTSYS code (which uses the discrete ordinates method) is 1.212945. FDM S_N, SP_3 and diffusion results were calculated using a discretization of 30x30 mesh. Table 9 shows the results for the multiplication

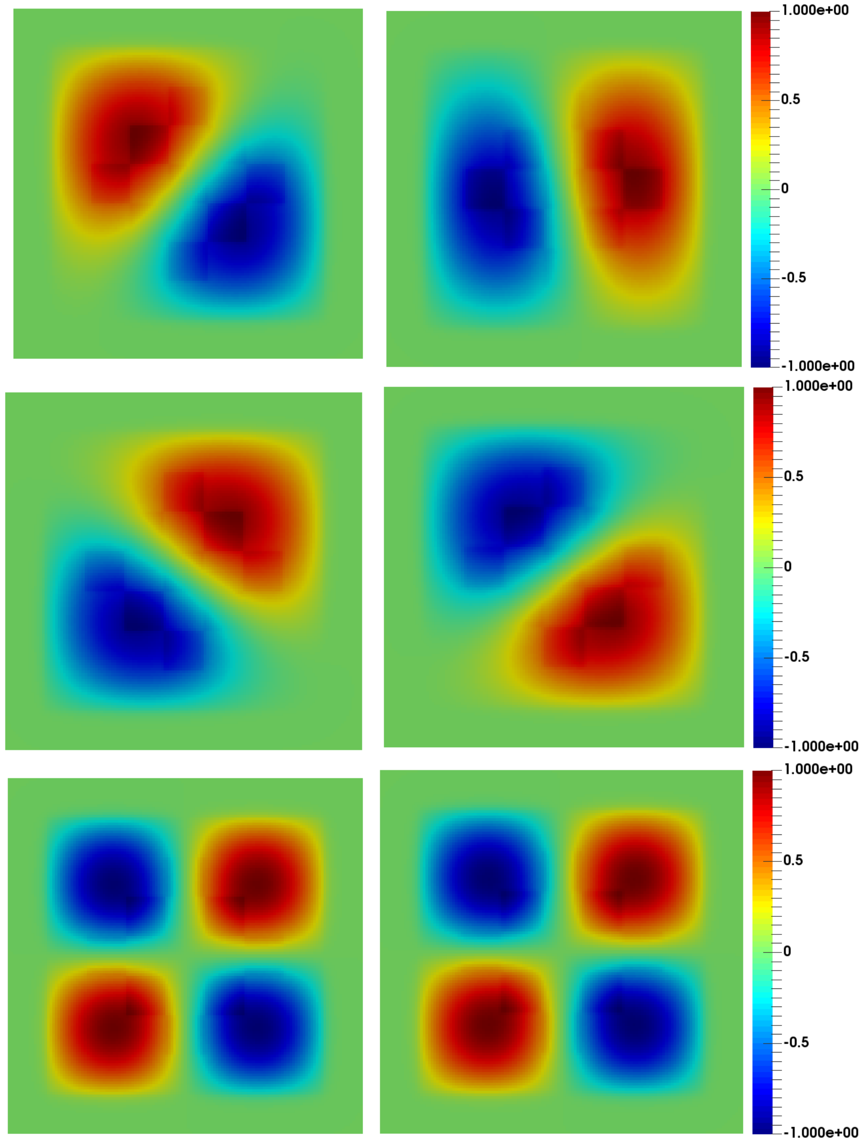

Figure 12: MOX: Normalized Scalar flux distribution for 2^{nd}, 3^{rd} and 4^{th} modes, FDM SP_3^C on the left, FDM S_8 on the right.

factor k_{eff}. A flux comparison between S_8, SP_3 and SP_1(Diffusion) can be seen in fig.14. Fig.15 shows the first group flux neutron distribution for the four dominant modes. It is easy to see that the cell-centered scheme SP_3 shows better results for the eigenvalue and for the flux distribution than diffusion or edge-centered SP_3. Another interesting observation is that the accuracy of the

SP_3 solution seems to be approximately the same as the S_4 method. Both differ considerably with respect to the S_8 solution, but it is helpful to understand intuitively that SP_3 solutions have approximately the same accuracy as S_4 solutions for at least some problems which are not highly diffusive. An important conclusion extracted from this sample is that it suggests that the shape of the lambda modes probably are insensitive to the angular approximation.

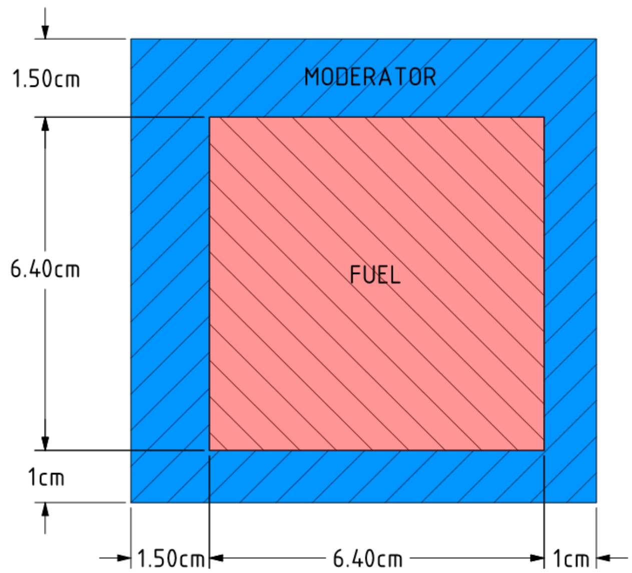

Figure 13: BWR cell problem geometry.

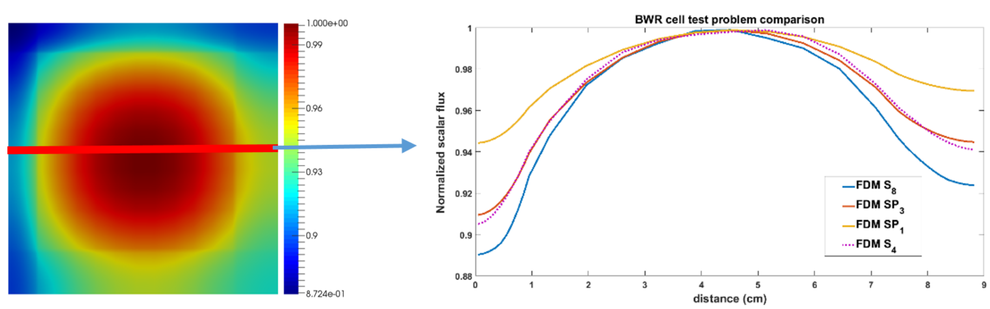

Figure 14: BWR cell test: scalar flux distribution for 1^{st} eigenvalue, 1^{st} energy group

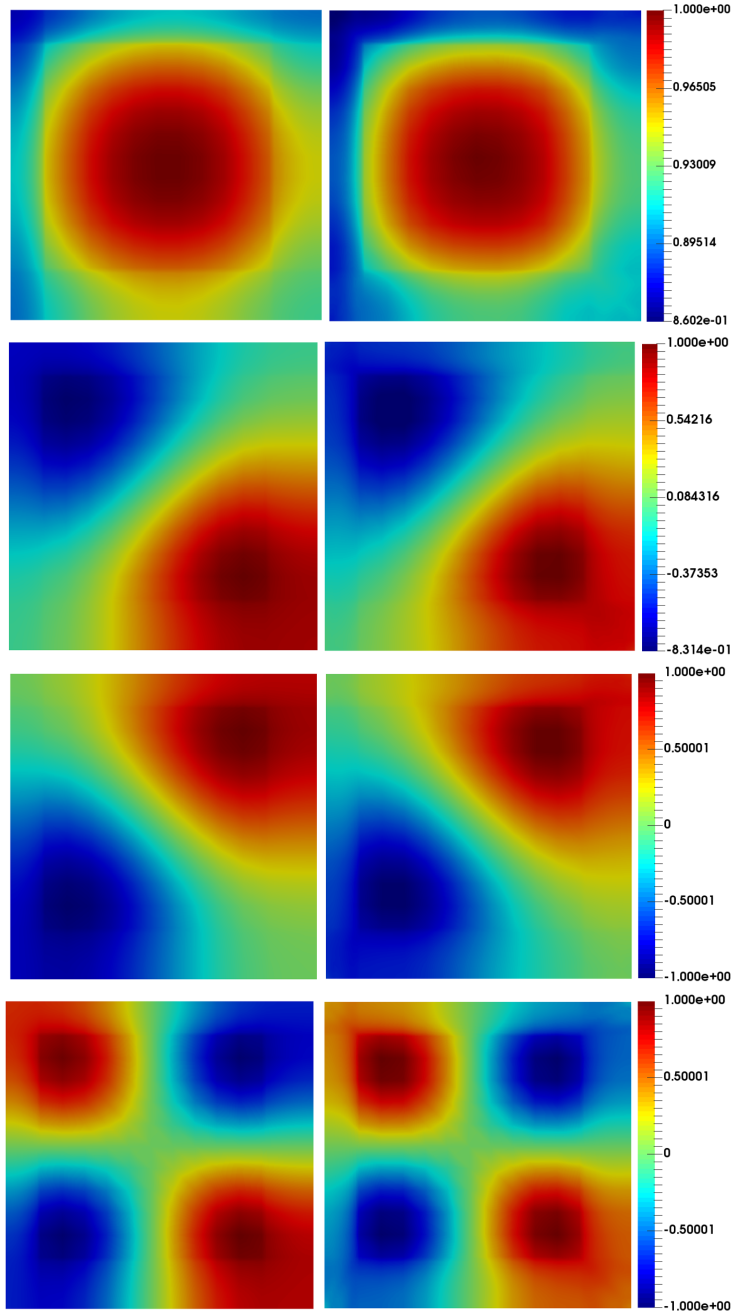

Figure 15: Four dominant eigenfunctions normalized first group flux distribution for the BWR cell benchmark problem. FDM SP_3 on the left, FDM S_8 on the right.

Table 8: BWR cell cross-sections. Thermal group is g=2.

Material	Group	Σ_t	$\nu\Sigma_f$	$\Sigma_{s,1\to g}$	$\Sigma_{s,2\to g}$	χ_g
Fuel	1	0.196647	0.006203	0.178000	0.001089	1.000
	2	0.596159	0.1101	0.010020	0.525500	0.000
Moderator	1	0.222064	0.000	0.199500	0.001558	0.000
	2	0.887874	0.000	0.021880	0.878300	0.000

Table 9: BWR cell benchmark K_{eff} results.

	Order	K_{eff}	pcm (ΔK_{eff})
DANTSYS	S_8	1.212945	-
FDM Sn	S_8	1.212944	0
FDM SP_3^C	-	1.213237	24
FDM $Dif.^C$	-	1.220100	589
FDM SP_3^E	-	1.214459	124
FDM $Dif.^E$	-	1.220886	654

3.5. Two-dimensional C5G7 test problem

PWR C5G7 MOX fuel assembly benchmark corresponds to a quarter symmetry core problem [17]. It is composed of water reflector region and 4 fuel elements surrounded by water, as seen in fig.16. The boundary conditions are vacuum and reflective, also shown in fig16. A 17×17 square pitch array of cylindrical fuel pins forms each fuel assembly. Since, in this work, the developed codes FDM SP_3 and FDM S_N are limited to the use of Cartesian geometry, the cylindrical pin is approximated by a square with the same area as the corresponding cylinder. Fig.17 corresponds to this approximation. Four different meshes are considered for the core, they can be seen in fig.18. The 7 energy groups cross-sections can be found in the benchmark [17] for the seven corresponding materials. To compose the reactor are considered three MOX pin fuels with different enrichments, UO_2 fuels, guide tubes, fission chambers and moderator. Table 12 summarize the comparison of results obtained by FDM Diffusion and FDM SP_3 with FEM SP_3 [18], FDM S_4 [11] and those obtained by MCNP, which provides the reference solution. Furthermore, k_{eff} values have been compared in the table 10 for all the meshes. Some important aspects can be extracted from the results: k_{eff} values calculated with edge-centered scheme shows better accuracy than those obtained by cell-centered scheme, although the maximum percentage error of the power calculated using cell-centered scheme shows lower values than those obtained by the edge-centered approach. Another observation here is that for coarse spatial mesh, the edge-centered scheme has better error cancellation than the cell-centered scheme. An analysis of the mesh influence is shown in tables 10 and 11. The increase of the number of cells is related with a high accuracy regarding to k_{eff} calculated with cell-centered scheme but no necessarily regarding to the power error. Fig. 19 shows the neutron flux distribution of the first eigenvalue for energy groups 1 and 7. Power distribution of C5G7 problem obtained by FDM SP_3 is represented in fig.20. Fig.21 shows eigenfluxes comparison between FDM SP_3 and FDM S_4. It can be appreciated that FDM S_4 eigenfluxes show a little ray effect compared with FDM SP_3.

Table 10: k_{eff} and Power comparison using cell-centered Scheme.

	Discret.	N of el.	k_{eff}	pcm	Max.Perc.Error	AVG	RMS	MRE
MCNP	-	-	1.186550	-	-	-	-	-
SP_3	1x1	17424	1.180898	476	7.380	2.665	2.923	2.512
$Dif.$	1x1	17424	1.182095	375	6.480	2.326	2.669	2.105
SP_3	4x4	191844	1.182067	377	5.666	2.463	2.654	2.331
$Dif.$	4x4	191844	1.183066	294	7.385	2.223	2.807	2.015
SP_3	6x6	412164	1.182089	375	5.699	2.506	2.691	2.380
$Dif.$	6x6	412164	1.183032	296	7.748	2.258	2.867	2.050
SP_3	8x8	715716	1.183621	247	5.846	2.414	2.642	2.297
$Dif.$	8x8	715716	1.183935	220	8.280	2.298	2.957	2.080

Table 11: k_{eff} and Power comparison using edge-centered scheme.

	Discret.	N of el.	k_{eff}	pcm	Max.Perc.Error	AVG	RMS	MRE
MCNP	-	-	1.186550	-	-	-	-	-
SP_3	1x1	17689	1.185380	99	6.537	2.116	2.652	1.983
$Dif.$	1x1	17689	1.184963	134	11.368	2.560	3.397	2.204
SP_3	4x4	192721	1.184884	140	5.685	2.190	2.533	2.217
$Dif.$	4x4	192721	1.184574	167	10.199	2.356	3.129	2.092
SP_3	6x6	413449	1.184468	175	5.655	2.246	2.544	2.193
$Dif.$	6x6	413449	1.184347	186	9.923	2.345	3.094	2.105
SP_3	8x8	717409	1.183928	221	5.746	2.396	2.644	2.334
$Dif.$	8x8	717409	1.184132	204	9.683	2.381	3.097	2.158

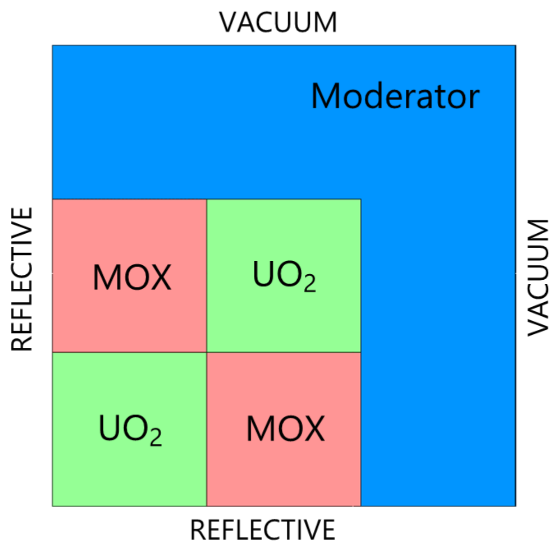

Figure 16: Assembly.

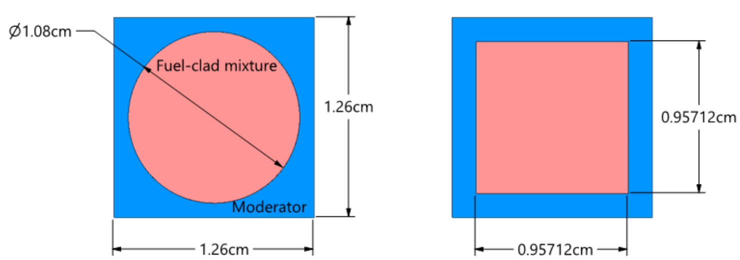

Figure 17: Pin cell approximation.

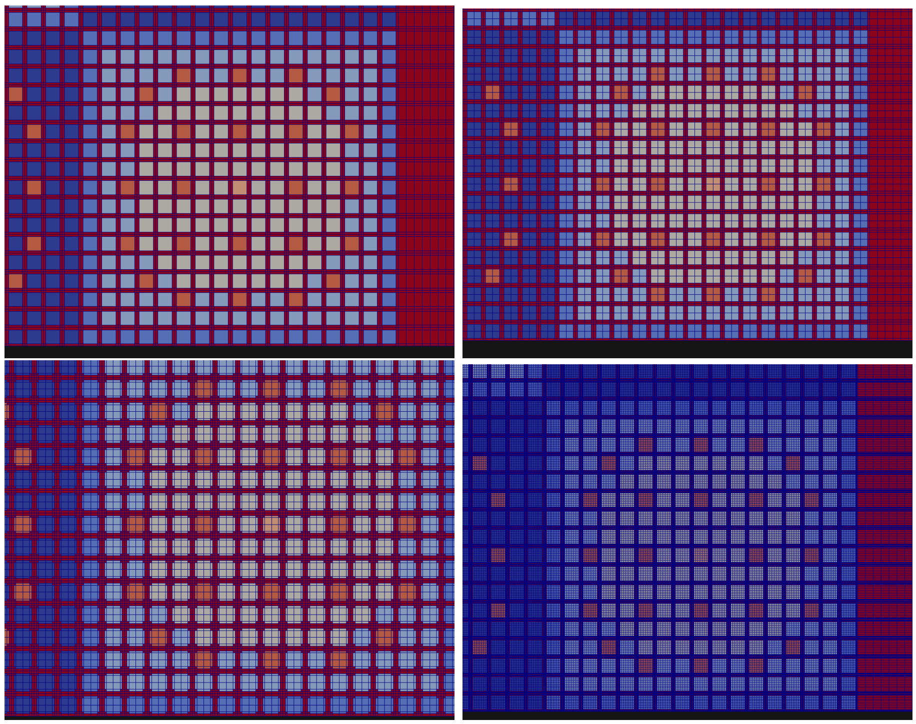

Figure 18: Detail of 1x1, 4x4, 6x6 and 8x8 meshes.

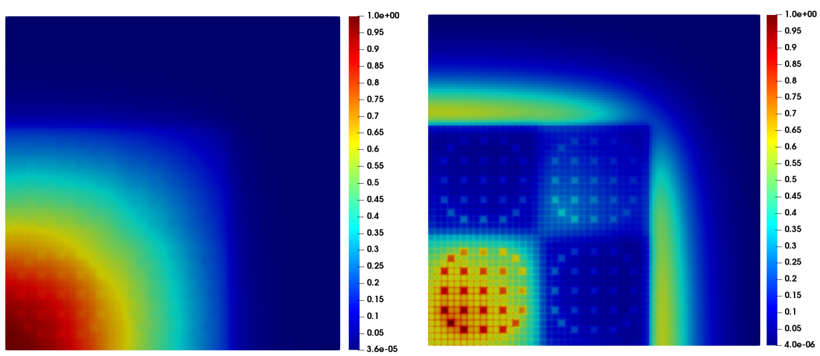

Figure 19: 1st eigenvalue FDM SP_3 flux distibution for 1 and 7 energy groups.

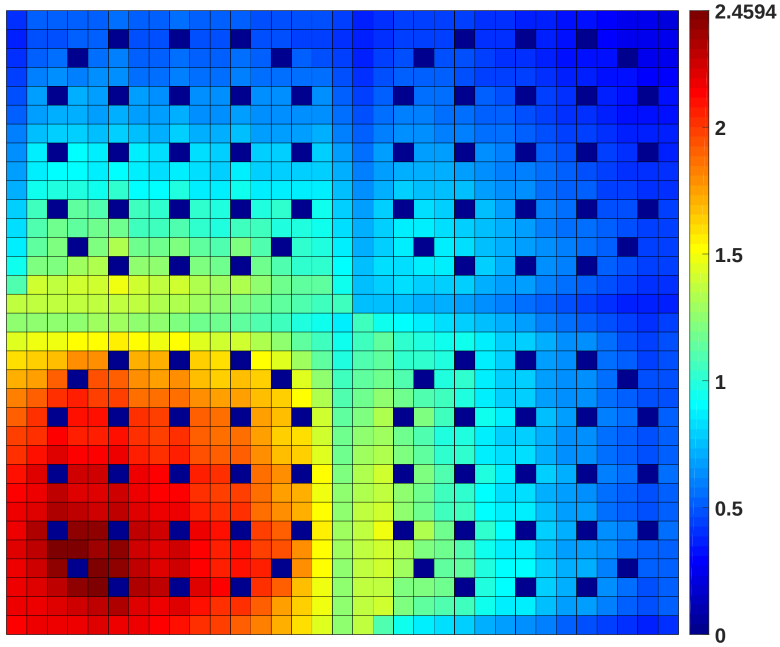

Figure 20: Power Distribution of C5G7 problem.

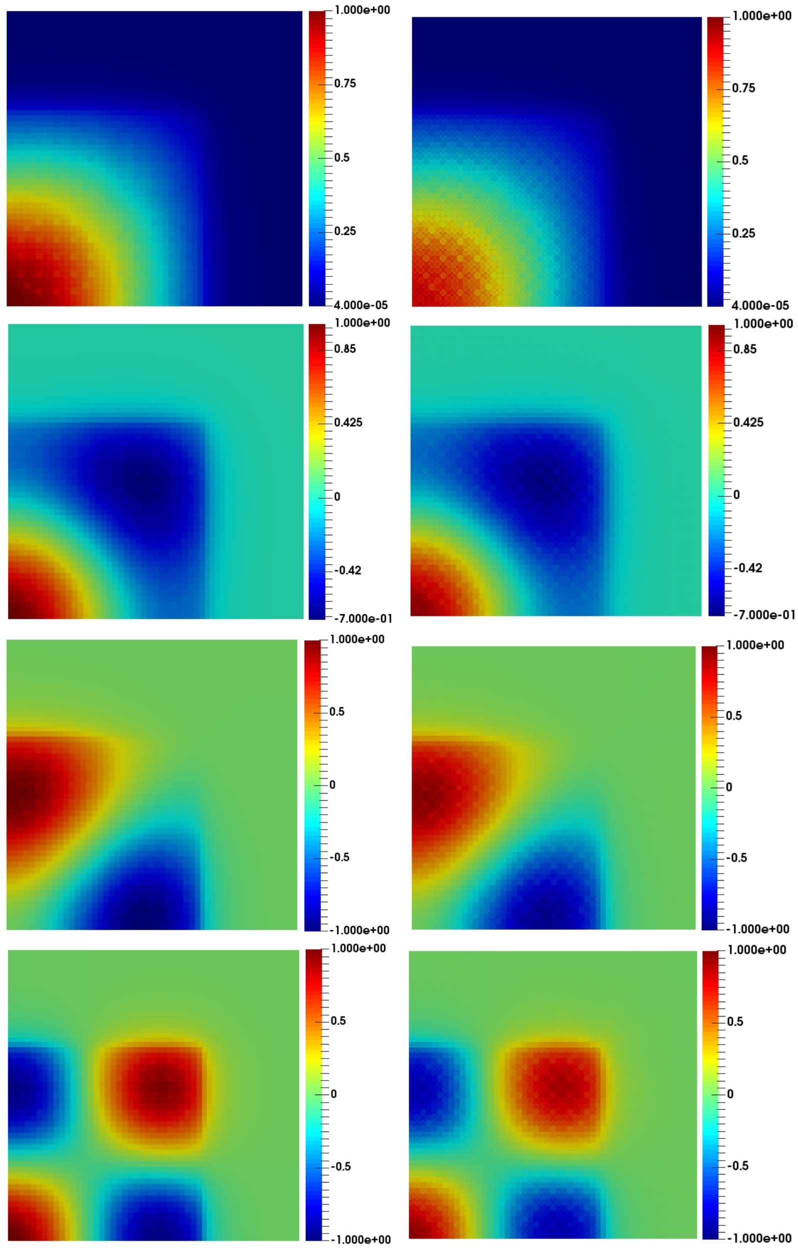

Figure 21: Shape and order of the four dominant eigenvectors for the first energy group are independent of the angular approximation. FDM SP_3 on the left, FDM S_4 on the right

Table 12: C5G7 Test problem results. *Results from [18].

	size	K_{eff}	pcm	Max. Perc. Error	Average Error	Mean Rel. Error	Avg.Pin Power	Max.Pin Power	Min.Pin Power	UO_2-1 Avg.Pin Power	MOX Avg.Pin Power	UO_2-2 Avg.Pin Power
MCNP Ref.		1.186550	-	-	-	-	1.000	2.498	0.232	1.867	0.802	0.529
FDM SP_3^C	1x1	1.180898	476	7.380	2.665	2.512	1.000	2.436	0.224	1.831	0.827	0.515
FDM SP_3^C	4x4	1.182067	377	5.666	2.463	2.331	1.000	2.455	0.227	1.835	0.825	0.515
FDM SP_3^C	6x6	1.182089	375	5.699	2.506	2.380	1.000	2.456	0.228	1.834	0.826	0.516
FDM SP_3^C	8x8	1.183621	247	5.846	2.414	2.297	1.000	2.461	0.230	1.835	0.825	0.515
FDM $Dif.^C$	1x1	1.182095	375	6.480	2.326	2.105	1.000	2.461	0.229	1.841	0.823	0.513
FDM $Dif.^C$	4x4	1.183066	293	7.385	2.223	2.015	1.000	2.473	0.232	1.842	0.822	0.514
FDM $Dif.^C$	6x6	1.183032	296	7.748	2.258	2.050	1.000	2.473	0.233	1.842	0.822	0.514
FDM $Dif.^C$	8x8	1.183935	220	8.280	2.298	2.080	1.000	2.475	0.234	1.841	0.822	0.514
*FEM SP_3		1.183470	260	-	0.810	0.720	-	-	-	-	-	-
FDM S_4	1x1	1.187600	88	6.745	2.110	1.802	1.000	2.515	0.2230	1.852	0.817	0.514

3.6. 3D Homogeneous Reactor

The 3D homogenized problem consist of a 100 cm x 60 cm x 180 cm in x,y, and z axis parallelepiped. Only one material is considered for this problem with the 2 energy-group cross sections presented in table 13, without up-scattering and with fission neutrons produced in the first energy group. Two different meshes are used in the simulation. The first mesh (mesh 1) is 24 x 16 x 38, the total number of elements is 14592. The second one (mesh 2) is 60 x 36 x 102, the total number of elements is 220320. Both meshes are shonw in fig.22. Vacuum boundary conditions are applied. The reference is PARTISN using a S_{16} order for the transport equations and using mesh 2. The multiplication factors are compared in table 14 and results obtained with FDM diffusion method are also added. Fig.23 shows the flux distribution of the first group. It is easy to see that values obtained by using mesh 2 and SP_3 solver, shows more accurate k_{eff} values taking as a reference the S_{16} solution.

Table 13: Cross-sections of the 3D homogeneous problem. Thermal energy group is g=2.

Group	Σ_t	$\nu\Sigma_f$	$\Sigma_{s,1\to g}$	$\Sigma_{s,2\to g}$	χ_g
1	$5.2096647 \cdot 10^{-1}$	$7.72686955 \cdot 10^{-3}$	$4.95171815 \cdot 10^{-1}$	-	1.0
2	1.31245720	$1.55083969 \cdot 10^{-1}$	$1.60585809 \cdot 10^{-2}$	1.20309806	0.0

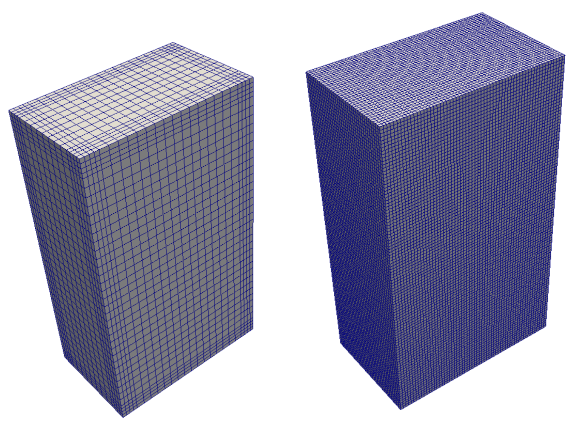

Figure 22: Homogeneous reactor meshes.

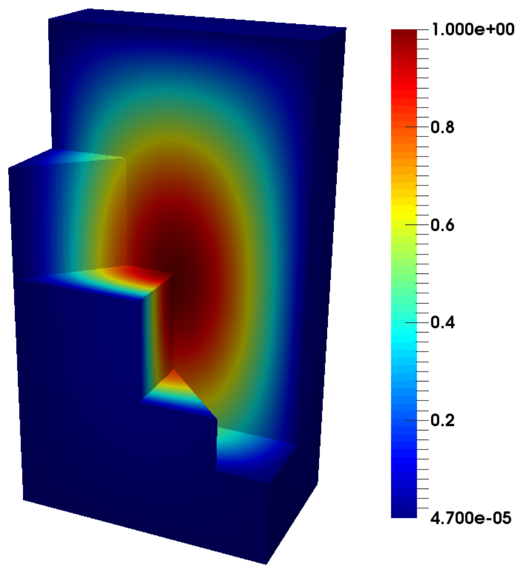

Figure 23: Homogeneous reactor flux distribution for eigenvalue 1.

Table 14: Multiplication factors for Homogeneous 3D problem.

	Order	K_{eff}	pcm (ΔK_{eff})
Reference PARTISN mesh2	S_{16}	1.074001	-
FDM SP_3^C mesh1	-	1.074696	64
FDM SP_3^C mesh2	-	1.074141	13
FDM $Dif.^C$ mesh 1	-	1.073891	10
FDM $Dif.^C$ mesh 2	-	1.073373	58
FDM SP_3^E mesh1	-	1.075042	96
FDM SP_3^E mesh2	-	1.074001	0
FDM $Dif.^E$ mesh 1	-	1.074592	55
FDM $Dif.E$ mesh 2	-	1.073342	61

3.6.1. Boundary conditions comparison

This section shows the differences between the three vacuum boundary approaches explained in section 2.2.1, 2.2.2 and 2.2.3, for the three-dimensional homogeneous problem.

As can be seen in table 15, the exact solution is only achieved with the third vacuum boundary condition approach (BC3). The second approach (BC2) differs from exact solution only in few decimals, while the first approach (BC1) differs considerably. All the results were calculated with the same discretization.

Table 15: First 4 eigenvalues for a 3D homogeneous problem SP3, boundary condition approaches comparison. *(SP_3^C is the SP_3 code using cell-centered scheme and BC refers to each boundary condition approach.)*

Eig.	FDM SP_3^C BC3	FDM SP_3^C BC2	FDM $SP_3^C BC1$
1st	1.074696	1.074525	1.067359
2nd	1.049500	1.050803	1.041714
3rd	1.010194	1.013610	1.001778
4th	1.006673	1.006186	0.996885

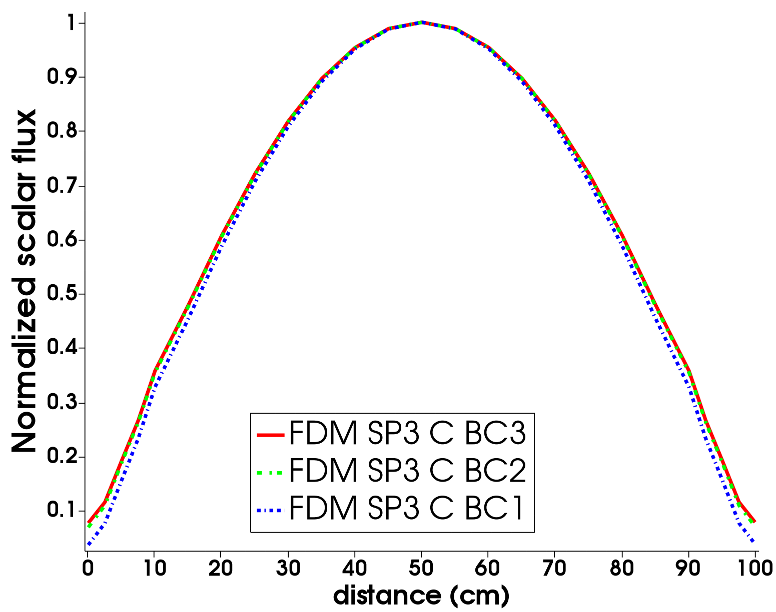

Figure 24: Normalized Scalar Flux for Homogeneous 3D reactor for a central line in x axis.

Figs.24, 25 and 26 show the normalized scalar flux calculated with the three different boundary condition approaches. In this case, the difference between the normalized scalar fluxes calculated with the three approaches is not negligible.

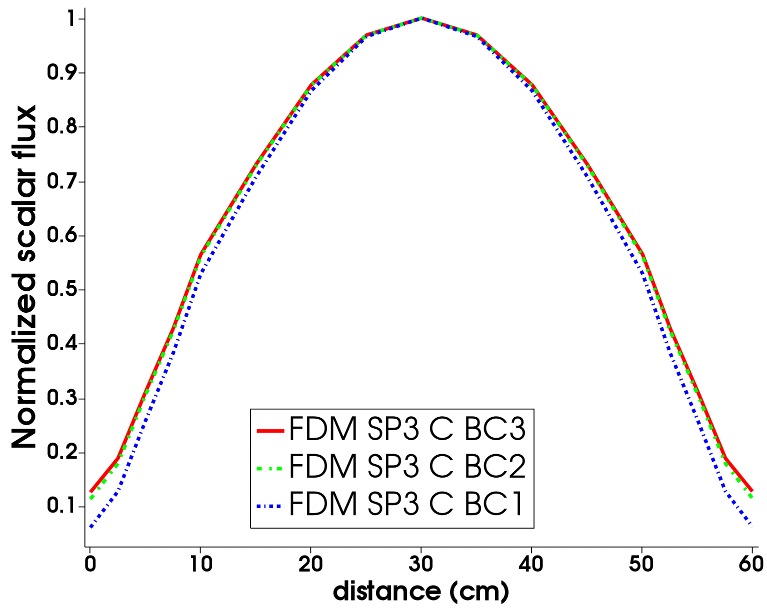

Figure 25: Normalized Scalar Flux for Homogeneous 3D reactor for a central line in y axis.

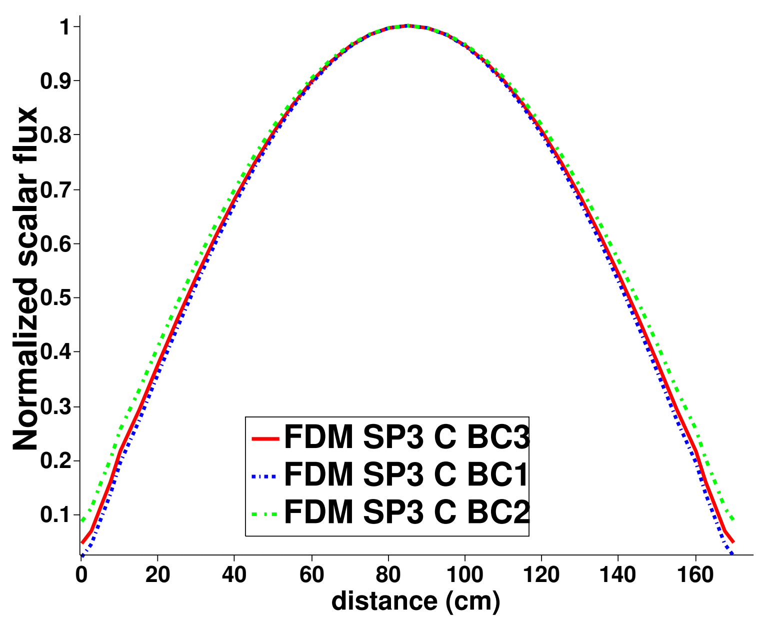

Figure 26: Normalized Scalar Flux for Homogeneous 3D reactor for a central line in z axis.

3.7. FBR Takeda Benchmark

The problem considered in this section is a small core model of a Fast Breeder Reactor (FBR). The model is generated with 4 energy groups, and the cross sections are given in [19]. The dimensions of the problem are 140 cm x 140 cm x 150 cm. The problem is composed of a fuel region, radial and axial blankets and control rod region. In [19] the problem is generated with symmetry conditions, however in this work the complete problem is considered like in [20]. Vacuum boundary conditions are applied. Fig.27 shows the mesh used (144 x 112 x 120). Two cases of the problem are considered. Case 1: control rods out. Case2: control rods half-inserted. A comparison of the multiplication factors, where the reference value was obtained with Monte Carlo method, is shown in table 16. FDM Diffusion result is also added in the comparison table. Figs.28 and 29 show the fluxes distribution of the first energy group for cases 1 and 2. Table 16 shows better results for the SP_3 cell-centered scheme compared with edge-centered scheme and Diffusion. Figs.30 and 31 show the fluxes distribution of the fourth energy group for cases 1 and 2.

Table 16: Multiplication factors for FBR problem.

	K_{eff} CASE 1	K_{eff} CASE 2
Reference Monte-Carlo	0.973620	0.959850
FDM SP_3^C	0.964604	0.951345
FDM $Dif.^C$	0.959346	0.945454
FDM SP_3^E	0.961727	0.947631
FDM $Dif.^E$	0.956340	0.941707

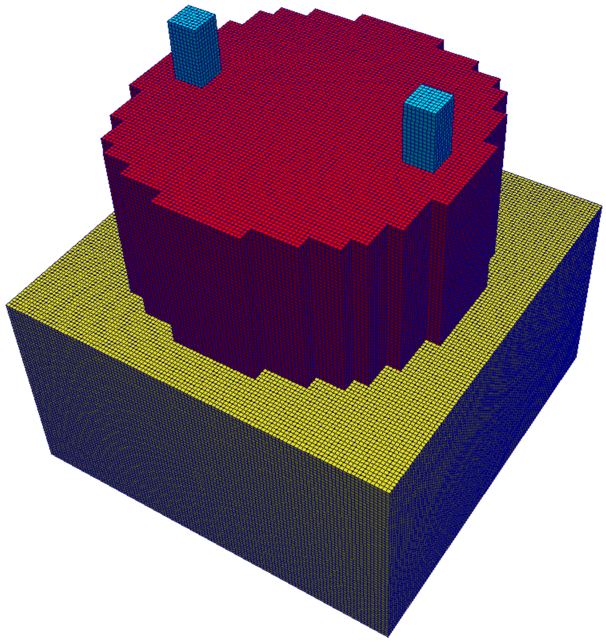

Figure 27: FBR reactor discretization (interior visualization of the reactor upper part).

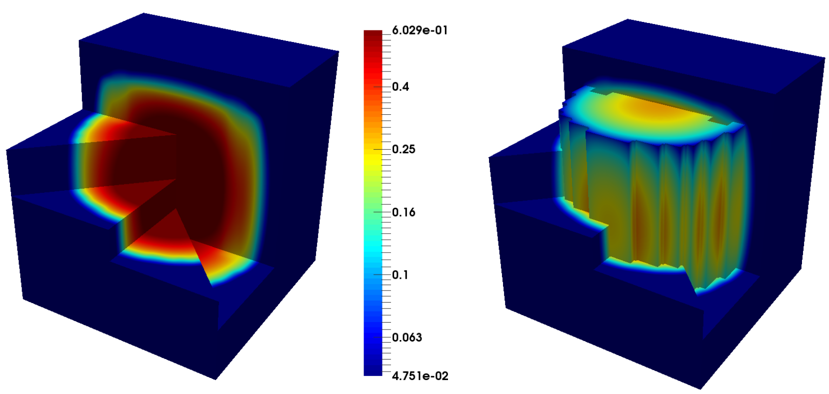

Figure 28: Case 1: FBR reactor flux distribution for group 1.

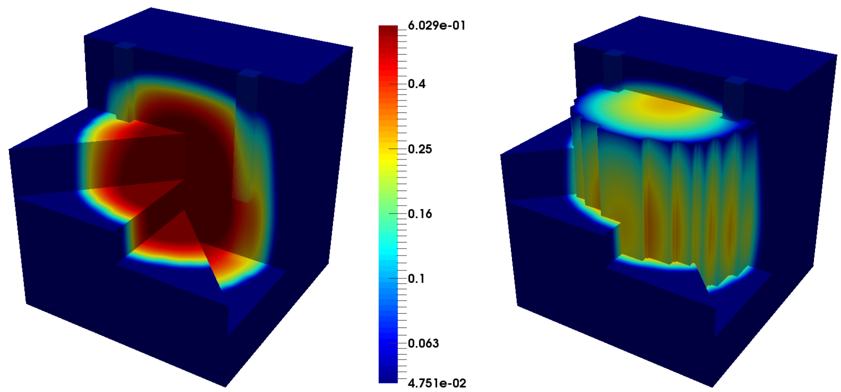

Figure 29: Case 2: FBR reactor flux distribution for group 1.

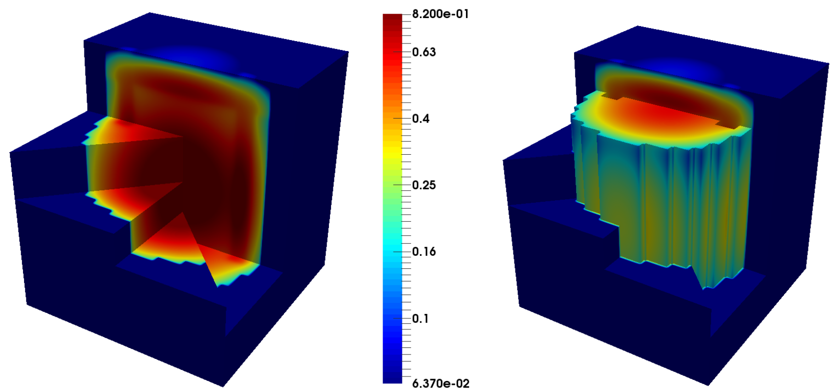

Figure 30: Case 1: FBR reactor flux distribution for group 4.

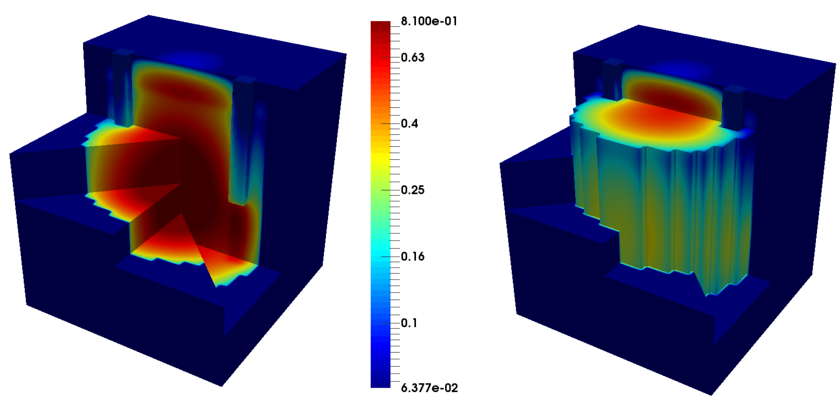

Figure 31: Case 2: FBR reactor flux distribution for group 4.

4. Conclusions

This work presents a method for solving the multidimensional steady-state multi-group Simplified Spherical Harmonics Equations using Cartesian geometry. Spatial discretization were performed by means of two versions of the Finite Difference Method. This method is capable of calculating multiple eigenvalues and eigenvectors with a simple formulation. The algorithms were programmed in a FORTRAN code called *SHE3NA*. This program has been validated with multiple one-dimensional, two-dimensional and three-dimensional benchmarks. The methods developed in this work shows that *SHE3NA* results have a good agreement with reference values.

A complete review of the SP_3 has been explained as well as a boundary condition study for both finite difference approximations used to spatial discretization. We also present the correct derivation of the finite difference vacuum boundary condition for SP_3, that the authors could not find elsewhere in the literature. We also show, that one may reasonably derive approximate boundary conditions that lead to solutions very close to those with correct ones. For these cases it may be difficult to identify the source of the error as it is quite small and easily attributable to incorrect sources (such as spatial discretization errors from a mesh that is not fully refined). Therefore, this work is valuable in presenting the correct finite difference vacuum boundary conditions and evaluation of some test problems to verify correct vacuum boundary conditions.

It can be appreciated with the results shown in previous sections that there exist important neutron flux differences between the three methods implemented: Diffusion, SP_3 and S_N. The work shows several numerical results, giving examples of problems in which Diffusion and SP_3 present good results, such us MOX or C5G7 problems, although S_N method is always more accurate. The results suggest that in small problems where the heterogeneities and the neutronic gradient are high, the SP_3 method gives similar results to discrete ordinates method and diffusion approximation is far from the neutron transport solution. The SP_3 method have similar accuracy to the S_4 method, and maybe it would mean that SP_5 could be approximately the same accuracy as S_8. So, it is important to know what method is suitable depending on the calculation and accuracy desired.

Another important conclusion is that the results suggest that the shape and order of the dominant eigenvectors are not affected by the chosen angular approximation.

Future works will be focused on the analysis of the SP_3 solver comparing different eigenvalue problem solvers and on the development of solutions for nonmultiplying systems which consider different type of particles (photons) in fixed source problems, which are could be useful in shielding and radiation protection.

Appendix A: Cell-Centered Finite Difference Method

Using the Fick's Law the current can be defined as:

$$J_g^0(x) = -D_g(x)^0 \frac{\partial \Phi_g(x)}{\partial x}, \qquad D_g(x)^0 = D_g(x). \tag{A.1}$$

So, eq.3 can be reformulated as:

$$\begin{aligned} &\frac{\partial}{\partial x} J_g^0(x) + \Sigma_{r,g}(x)\Phi_g(x) = \\ &\quad \frac{\chi_g(x)}{K_{eff}} \sum_{g'} \nu \Sigma_{f,g'}(x)\phi_{g'}^0(x) + \sum_{g' \neq g} \Sigma_{s,g' \to g}(x)\phi_{g'}^0(x) + 2\Sigma_{r,g}(x)\phi_g^2(x), \end{aligned} \tag{A.2}$$

Considering the cell-centered finite difference approach:

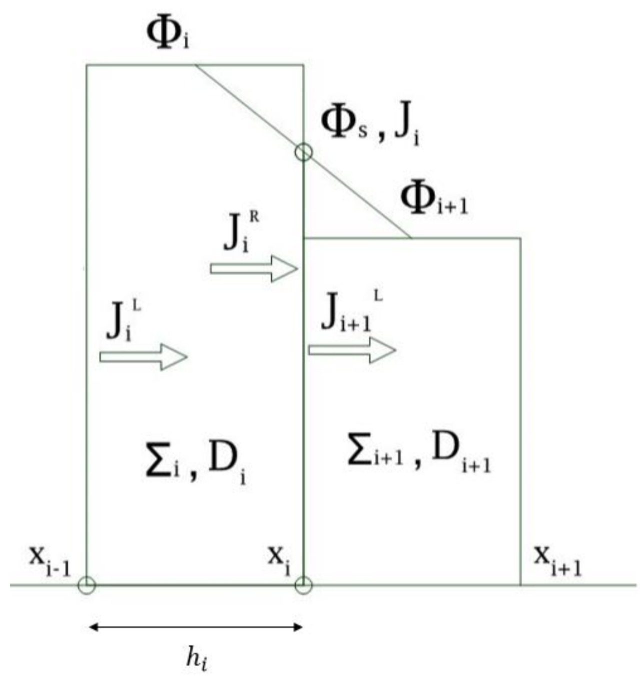

Figure A.1: Cell-centered Finite Difference

$$\begin{aligned} J_{g,i}^0 - J_{g,i-1}^0 + \int_{x_{i-1}}^{x_i} \Sigma_{r,g}(x)\Phi_g(x)dx = \frac{\chi_g(x)}{K_{eff}} \int_{x_{i-1}}^{x_i} \sum_{g'} \nu \Sigma_{f,g'}(x)\phi_{g'}^0(x)dx + \\ \int_{x_{i-1}}^{x_i} \sum_{g' \neq g} \Sigma_{s,g' \to g}(x)\phi_{g'}^0(x)dx + 2\int_{x_{i-1}}^{x_i} \Sigma_{r,g}(x)\phi_g^2(x)dx, \end{aligned} \tag{A.3}$$

where:

$$\int_{x_{i-1}}^{x_i} \Sigma_{r,g}(x)\Phi_g(x)dx = \Sigma_{r,g}(x)\int_{x_{i-1}}^{x_i} \Phi_g(x)dx = \Sigma_{r,i,g}h_i\Phi_{i,g}, \tag{A.4}$$

$$\int_{x_{i-1}}^{x_i} \sum_{g'} \nu\Sigma_{f,g'}(x)\phi^0_{g'}(x)dx = \sum_{g'} \nu\Sigma_{f,i,g'}h_i\phi^0_{i,g'}, \tag{A.5}$$

$$\int_{x_{i-1}}^{x_i} \sum_{g'\neq g} \Sigma_{s,g'\to g}(x)\phi^0_{g'}(x)dx = \sum_{g'\neq g} \Sigma_{s,i,g'\to g}h_i\phi^0_{i,g'}, \tag{A.6}$$

$$\int_{x_{i-1}}^{x_i} \Sigma_{r,g}(x)\phi^2_g(x)dx = \Sigma_{r,i,g}h_i\phi^2_{i,g}, \tag{A.7}$$

$$\Phi_{i,g} = \frac{1}{h_i}\int_{x_{i-1}}^{x_i} \Phi_g(x)dx, \tag{A.8}$$

This allows eq.A.2 to be written in the form:

$$\begin{aligned} &J^0_{i,g} - J^0_{i-1,g} + \Sigma_{r,i,g}h_i\Phi_{i,g} = \\ &\qquad \frac{\chi_{i,g}}{K_{eff}}\sum_{g'} \nu\Sigma_{f,i,g'}h_i\phi^0_{i,g'} + \sum_{g'\neq g} \Sigma_{s,i,g'\to g}h_i\phi^0_{i,g'} + 2\Sigma_{r,i,g}h_i\phi^2_{i,g}, \end{aligned} \tag{A.9}$$

Taking into account the present cell-centered finite difference scheme we can define:

$$J^{0,R}_{i,g}(x) = -D^0_{i,g}(x)\frac{\partial\Phi_g(x)}{\partial x}, \tag{A.10}$$

$$J^{0,R}_{i,g} = -D^0_{i,g}\frac{\Phi^R_{i,g} - \Phi_{i,g}}{h_i/2}, \tag{A.11}$$

$$J^{0,L}_{i+1,g} = -D^0_{i+1,g}\frac{\Phi_{i+1,g} - \Phi^L_{i+1,g}}{h_{i+1}/2}, \tag{A.12}$$

with the interface conditions:

$$J^{0,R}_i = J^{0,L}_{i+1} = J^0_i, \tag{A.13}$$

$$\Phi^R_i = \Phi^L_{i+1} = \Phi_s. \tag{A.14}$$

Then, from eq.A.13 :

$$-D^0_{i,g}\frac{\Phi_{s,g} - \Phi_{i,g}}{h_i/2} = -D^0_{i+1,g}\frac{\Phi_{i+1,g} - \Phi_{s,g}}{h_{i+1}/2}, \tag{A.15}$$

$$\Phi_{s,g} = \frac{D^0_{i,g}/h_i}{D^0_{i,g}/h_i + D^0_{i+1,g}/h_{i+1}}\Phi_{i,g} + \frac{D^0_{i+1,g}/h_{i+1}}{D^0_{i,g}/h_i + D^0_{i+1,g}/h_{i+1}}\Phi_{i+1,g} = \omega^0_{i,g}\Phi_{i,g} + (1-\omega^0_{i,g})\Phi_{i+1,g}. \quad (A.16)$$

Then, substituting eq.A.16 into eq.A.11 the currents of the eq.A.9 can be expressed as:

$$J^0_{i,g} = J^{0,R}_{i,g} = -\widetilde{D}^0_{i,g}(\Phi_{i+1,g} - \Phi_{i,g}), \quad (A.17)$$

$$J^0_{i-1,g} = J^{0,L}_{i,g} = -\widetilde{D}^0_{i-1,g}(\Phi_{i,g} - \Phi_{i-1,g}), \quad (A.18)$$

where:

$$\widetilde{D}^0_{i,g} = \frac{2D^0_{i,g}D^0_{i+1,g}}{D^0_{i,g}h_{i+1} + D^0_{i+1,g}h_i}, \quad (A.19)$$

$$\widetilde{D}^0_{i-1,g} = \frac{2D^0_{i-1,g}D^0_{i,g}}{D^0_{i-1,g}h_i + D^0_{i,g}h_{i-1}}. \quad (A.20)$$

Finally, eq.A.9 is re-written as a discretized mesh balance equation as follows:

$$-\widetilde{D}^0_{i-1,g}\Phi_{i-1,g} + [\widetilde{D}^0_{i-1,g} + \widetilde{D}^0_{i,g} + \Sigma_{r,i,g}h_i]\Phi_{i,g} - \widetilde{D}^0_{i,g}\Phi_{i+1,g} = \frac{\chi_{i,g}}{K_{eff}}\sum_{g'}\nu\Sigma_{f,i,g'}h_i\phi^0_{i,g'} + \sum_{g'\neq g}\Sigma_{s,i,g'\to g}h_i\phi^0_{i,g'} + 2\Sigma_{r,i,g}h_i\phi^2_{i,g}. \quad (A.21)$$

The same procedure can be followed for the eq.4. Considering the Fick's Law:

$$J^2_g(x) = -D^2_g(x)\frac{\partial\phi^2_g(x)}{\partial x}, \qquad D^2_g(x) = \frac{27}{35}D_g(x). \quad (A.22)$$

Eq.4 takes the form:

$$\frac{\partial}{\partial x}J^2_g(x) + \Sigma_{t,g}(x)\phi^2_g(x) = \frac{2}{5}\Sigma_{r,g}(x)\phi^0_g(x) - \frac{2}{5}\frac{\chi_g(x)}{K_{eff}}\sum_{g'}\nu\Sigma_{f,g'}(x)\phi^0_{g'}(x) - \frac{2}{5}\sum_{g'\neq g}\Sigma_{s,g'\to g}(x)\phi^0_{g'}(x), \quad (A.23)$$

using cell-centered finite difference approximation:

$$J^2_{i,g} - J^2_{i-1,g} + \Sigma_{t,i,g}h_i\phi^2_{i,g} = \frac{2}{5}\Sigma_{r,i,g}h_i\phi^0_{i,g} - \frac{2}{5}\frac{\chi_{i,g}}{K_{eff}}\sum_{g'}\nu\Sigma_{f,i,g'}h_i\phi^0_{i,g'} - \frac{2}{5}\sum_{g'\neq g}\Sigma_{s,i,g'\to g}(x)h_i\phi^0_{i,g'}. \quad (A.24)$$

Then, the currents of the eq.A.24 can be expressed as:

$$J_{i,g}^2 = J_{i,g}^{2,R} = -\widetilde{D}_{i,g}^2(\phi_{i+1,g}^2 - \phi_{i,g}^2), \tag{A.25}$$

$$J_{i-1,g}^2 = J_{i,g}^{2,L} = -\widetilde{D}_{i-1,g}^2(\phi_{i,g}^2 - \phi_{i-1,g}^2), \tag{A.26}$$

where:

$$\widetilde{D}_{i,g}^2 = \frac{2D_{i,g}^2 D_{i+1,g}^2}{D_{i,g}^2 h_{i+1} + D_{i+1,g}^2 h_i}, \tag{A.27}$$

$$\widetilde{D}_{i-1,g}^2 = \frac{2D_{i-1,g}^2 D_{i,g}^2}{D_{i-1,g}^2 h_i + D_{i,g}^2 h_{i-1}}. \tag{A.28}$$

Finally, eq.A.24 is re-written as a discretized mesh balance equation as follows:

$$\begin{aligned}&-\widetilde{D}_{i-1,g}^2\phi_{i-1,g}^2 + [\widetilde{D}_{i-1,g}^2 + \widetilde{D}_{i,g}^2 + \Sigma_{t,i,g}h_i]\phi_{i,g}^2 - \widetilde{D}_{i,g}^2\phi_{i+1,g}^2 = \\ &\frac{2}{5}\Sigma_{r,i,g}h_i\phi_{i,g}^0 - \frac{2}{5}\frac{\chi_{i,g}}{K_{eff}}\sum_{g'}\nu\Sigma_{f,i,g'}h_i\phi_{i,g'}^0 - \frac{2}{5}\sum_{g'\neq g}\Sigma_{s,i,g'\to g}(x)h_i\phi_{i,g'}^0.\end{aligned} \tag{A.29}$$

The coupled SP_3 equations discretized using cell-centered Finite Difference method are:

$$\begin{aligned}&-\widetilde{D}_{i-1,g}^0\Phi_{i-1,g} + [\widetilde{D}_{i-1,g}^0 + \widetilde{D}_{i,g}^0 + \Sigma_{r,i,g}h_i]\Phi_{i,g} - \widetilde{D}_{i,g}^0\Phi_{i+1,g} = \\ &\qquad\frac{\chi_{i,g}}{K_{eff}}\sum_{g'}\nu\Sigma_{f,i,g'}h_i\phi_{i,g'}^0 + \sum_{g'\neq g}\Sigma_{s,i,g'\to g}h_i\phi_{i,g'}^0 + 2\Sigma_{r,i,g}h_i\phi_{i,g}^2,\end{aligned} \tag{A.30}$$

$$\begin{aligned}&-\widetilde{D}_{i-1,g}^2\phi_{i-1,g}^2 + [\widetilde{D}_{i-1,g}^2 + \widetilde{D}_{i,g}^2 + \Sigma_{t,i,g}h_i]\phi_{i,g}^2 - \widetilde{D}_{i,g}^2\phi_{i+1,g}^2 = \\ &\frac{2}{5}\Sigma_{r,i,g}h_i\phi_{i,g}^0 - \frac{2}{5}\frac{\chi_{i,g}}{K_{eff}}\sum_{g'}\nu\Sigma_{f,i,g'}h_i\phi_{i,g'}^0 - \frac{2}{5}\sum_{g'\neq g}\Sigma_{s,i,g'\to g}(x)h_i\phi_{i,g'}^0,\end{aligned} \tag{A.31}$$

where:

$$\widetilde{D}_{i,g}^m = \frac{2D_{i,g}^m D_{i+1,g}^m}{D_{i,g}^m h_{i+1} + D_{i+1,g}^m h_i}, \tag{A.32}$$

$$\widetilde{D}_{i-1,g}^m = \frac{2D_{i-1,g}^m D_{i,g}^m}{D_{i-1,g}^m h_i + D_{i,g}^m h_{i-1}}, \tag{A.33}$$

$$\begin{aligned} m &= 0, 2, \\ \Phi_{i,g} &= \phi_{i,g}^0 + 2\phi_{i,g}^2, \\ D_{i,g}^0 &= D_{i,g} = \frac{1}{3\Sigma_{t,i,g}}, \\ D_{i,g}^2 &= \frac{27}{35}D_{i,g}. \end{aligned}$$

Appendix B: Edge-Centered Finite Difference Method

Starting from the eq.A.2:

$$\frac{\partial}{\partial x} J_g^0(x) + \Sigma_{r,g}(x)\Phi_g(x) = \frac{\chi_g(x)}{K_{eff}} \sum_{g'} \nu\Sigma_{f,g'}(x)\phi^0_{g'}(x) + \sum_{g' \neq g} \Sigma_{s,g' \to g}(x)\phi^0_{g'}(x) + 2\Sigma_{r,g}(x)\phi^2_g(x),$$

and using finite difference edge-centered scheme approximation according to fig.B.1:

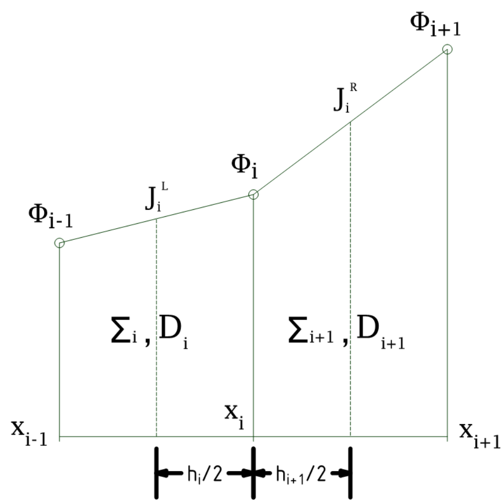

Figure B.1: Finite difference edge-centered scheme

$$J^{0,R}_{g,i} - J^{0,L}_{g,i} + \int_{x_{i-1}+h_i/2}^{x_i+h_{i+1}/2} \Sigma_{r,g}(x)\Phi_g(x)dx = \frac{\chi_g(x)}{K_{eff}} \int_{x_{i-1}+h_i/2}^{x_i+h_{i+1}/2} \sum_{g'} \nu\Sigma_{f,g'}(x)\phi^0_{g'}(x)dx + \int_{x_{i-1}+h_i/2}^{x_i+h_{i+1}/2} \sum_{g' \neq g} \Sigma_{s,g' \to g}(x)\phi^0_{g'}(x)dx + 2\int_{x_{i-1}+h_i/2}^{x_i+h_{i+1}/2} \Sigma_{r,g}(x)\phi^2_g(x)dx, \quad \text{(B.1)}$$

$$\int_{x_{i-1}+h_i/2}^{x_i+h_{i+1}/2} \Sigma_{r,g}(x)\Phi_g(x)dx \approx \Phi_g(x_i)\int_{x_{i-1}+h_i/2}^{x_i+h_{i+1}/2} \Sigma_{r,g}(x)dx = \frac{1}{2}(h_i\Sigma_{r,g,i} + h_{i+1}\Sigma_{r,g,i+1})\Phi_{g,i} = \overline{\Sigma}_{r,g,i}\Phi_{g,i}, \quad \text{(B.2)}$$

$$\int_{x_{i-1}+h_i/2}^{x_i+h_{i+1}/2} \sum_{g'} \nu\Sigma_{f,g'}(x)\phi^0_{g'}(x)dx \approx \sum_{g'} \frac{1}{2}(h_i\nu\Sigma_{f,i,g'} + h_{i+1}\nu\Sigma_{f,i+1,g'})\phi^0_{i,g'}$$
$$= \sum_{g'} \overline{\nu\Sigma}_{f,g,i}\phi^0_{i,g'}, \quad \text{(B.3)}$$

$$\int_{x_{i-1}+h_i/2}^{x_i+h_{i+1}/2} \sum_{g'\neq g} \Sigma_{s,g'\to g}(x)\phi^0_{g'}(x)dx \approx \sum_{g'\neq g} \frac{1}{2}(h_i\Sigma_{s,g'\to g,i}+h_{i+1}\Sigma_{s,g'\to g,i+1})\phi^0_{g',i}$$
$$= \sum_{g'\neq g} \overline{\Sigma}_{s,g'\to g,i}\phi^0_{g',i}, \quad \text{(B.4)}$$

$$\int_{x_{i-1}+h_i/2}^{x_i+h_{i+1}/2} \Sigma_{r,g}(x)\phi^2_g(x)dx \;\approx\; \frac{1}{2}(h_i\Sigma_{r,i,g} + h_{i+1}\Sigma_{r,i+1,g})\phi^2_{i,g} \;=\; \overline{\Sigma}_{r,g,i}\phi^2_{g,i}. \quad \text{(B.5)}$$

Eq.A.2 is transformed into eq.B.6

$$J^{0,R}_{g,i} - J^{0,L}_{g,i} + \overline{\Sigma}_{r,g,i}\Phi_{g,i} =$$
$$\frac{\chi_{g,i}}{K_{eff}} \sum_{g'} \overline{\nu\Sigma}_{f,g',i}\phi^0_{g',i} + \sum_{g'\neq g} \overline{\Sigma}_{s,g'\to g,i}\phi^0_{g',i} + 2\overline{\Sigma}_{r,g,i}\phi^2_{g,i}, \quad \text{(B.6)}$$

$$J^{0,R}_{g,i}(x) = -D^0_{g,i}(x)\frac{\partial\Phi_g(x)}{\partial x}, \quad \text{(B.7)}$$

$$J^{0,R}_{g,i} = -D^0_{g,i+1}\frac{\Phi_{g,i+1}-\Phi_{g,i}}{h_{i+1}/2}, \quad \text{(B.8)}$$

$$J^{0,L}_{g,i} = -D^0_{g,i}\frac{\Phi_{g,i}-\Phi_{g,i-1}}{h_i/2}. \quad \text{(B.9)}$$

Finally, eq.B.6 is re-written as a discretized mesh balance equation as follows:

$$\left[\frac{D^0_{g,i+1}}{h_{i+1}} + \frac{D^0_{g,i}}{h_i} + \overline{\Sigma}_{r,g,i}\right]\Phi_{g,i} - \frac{D^0_{g,i+1}}{h_{i+1}}\Phi_{g,i+1} - \frac{D^0_{g,i}}{h_i}\Phi_{g,i-1} - 2\overline{\Sigma}_{r,g,i}\phi^2_{g,i} =$$
$$\frac{\chi_{g,i}}{K_{eff}} \sum_{g'} \overline{\nu\Sigma}_{f,g',i}\phi^0_{g',i} + \sum_{g'\neq g} \overline{\Sigma}_{s,g'\to g,i}\phi^0_{g',i}, \quad \text{(B.10)}$$

Using the same procedure eq.A.23 can be expressed in a discretized way as:

$$\left[\frac{D^2_{g,i+1}}{h_{i+1}}+\frac{D^2_{g,i}}{h_i}+\overline{\Sigma}_{t,g,i}\right]\phi^2_{g,i}-\frac{D^2_{g,i+1}}{h_{i+1}}\phi^2_{g,i+1}-\frac{D^2_{g,i}}{h_i}\phi^2_{g,i-1}-\frac{2}{5}\overline{\Sigma}_{r,g,i}\phi^0_{g,i}=$$
$$-\frac{2}{5}\frac{\chi_{g,i}}{K_{eff}}\sum_{g'}\overline{\nu\Sigma}_{f,g',i}\phi^0_{g',i}-\frac{2}{5}\sum_{g'\neq g}\overline{\Sigma}_{s,g'\to g,i}\phi^0_{g',i}. \quad \text{(B.11)}$$

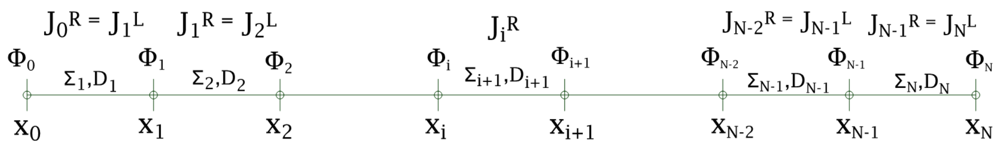

Figure B.2: Edge-centered Scheme

Acknowledgments

This work has been partially supported by the Spanish Agencia Estatal de Investigacion [grant number BES-2016-076782], the Spanish Ministerio de Economia Industria y Competitividad [project ENE2015-68353-P], [project ENE2017-89029-P-AR] and [project PGC2018-096437-B-I00-AR].

References

[1] K. D. Lathrop, B. G. Carlson, Discrete ordinates angular quadrature of the neutron transport equation, Tech. rep., Los Alamos Scientific Lab., N. Mex. (1964).

[2] E. M. Gelbard, Application of spherical harmonics method to reactor problems, Bettis Atomic Power Laboratory, West Mifflin, PA, Technical Report No. WAPD-BT-20.

[3] P. S. Brantley, E. W. Larsen, The simplified p 3 approximation, Nuclear Science and Engineering 134 (1) (2000) 1–21.

[4] S. P. Hamilton, T. M. Evans, Efficient solution of the simplified pn equations, Journal of Computational Physics 284 (2015) 155–170.

[5] K. Tada, A. Yamamoto, Y. Yamane, Y. Kitamuray, Applicability of the diffusion and simplified p3 theories for pin-by-pin geometry of bwr, Journal of nuclear science and technology 45 (10) (2008) 997–1008.

[6] E. W. Larsen, J. E. Morel, J. M. McGhee, Asymptotic derivation of the multigroup p1 and simplified pn equations with anisotropic scattering, Nuclear science and engineering 123 (3) (1996) 328–342.

[7] A. Vidal-Ferràndiz, S. González-Pintor, D. Ginestar, A. Carreño, G. Verdú, Optimized eigenvalue solvers for the neutron transport equation, in: International Conference on Computational Science, Springer, 2018, pp. 823–832.

[8] Á. Bernal, A. Hébert, J. E. Roman, R. Miró, G. Verdú, A krylov–schur solution of the eigenvalue problem for the neutron diffusion equation discretized with the raviart–thomas method, Journal of Nuclear Science and Technology 54 (10) (2017) 1085–1094.

[9] V. Hernandez, J. E. Roman, V. Vidal, Slepc: A scalable and flexible toolkit for the solution of eigenvalue problems, ACM Transactions on Mathematical Software (TOMS) 31 (3) (2005) 351–362.

[10] S. Balay, S. Abhyankar, M. F. Adams, J. Brown, P. Brune, K. Buschelman, L. Dalcin, A. Dener, V. Eijkhout, W. D. Gropp, D. Karpeyev, D. Kaushik, M. G. Knepley, D. A. May, L. C. McInnes, R. T. Mills, T. Munson, K. Rupp, P. Sanan, B. F. Smith, S. Zampini, H. Zhang, H. Zhang, PETSc users manual, Tech. Rep. ANL-95/11 - Revision 3.11, Argonne National Laboratory (2019).
URL `http://www.mcs.anl.gov/petsc`

[11] S. Morató, Á. Bernal, R. Miró, J. E. Roman, G. Verdú, Calculation of λ modes of the multi-group neutron transport equation using the discrete ordinates and finite difference method, Annals of Nuclear Energy 137 (2020) 107077.

[12] A. Vidal Ferràndiz, Development of a finite element method for neutron transport equation approximations, Ph.D. thesis (2018).

[13] M. Capilla, C. Talavera, D. Ginestar, G. Verdú, A nodal collocation approximation for the multi-dimensional pl equations–2d applications, Annals of Nuclear Energy 35 (10) (2008) 1820–1830.

[14] M. Capilla, C. Talavera, D. Ginestar, G. Verdú, A nodal collocation method for the calculation of the lambda modes of the pl equations, Annals of Nuclear Energy 32 (17) (2005) 1825–1853.

[15] J. Stepanek, T. Auerbach, W. Hälg, Calculation of four thermal reactor benchmark problems in xy geometry, Tech. rep., Eidgenoessisches Inst. fuer Reaktorforschung (1982).

[16] S. Kashi, A. Minuchehr, A. Zolfaghari, B. Rokrok, Mesh-free method for numerical solution of the multi-group discrete ordinate neutron transport equation, Annals of Nuclear Energy 106 (2017) 51–63.

[17] M. Smith, E. Lewis, B. Na, Benchmark on deterministic transport calculations without spatial homogenization: A 2-d/3-d mox fuel assembly 3-d benchmark (2003).

[18] A. Vidal-Ferrndiz, A. Carreo, D. Ginestar, G. Verd, A block arnoldi method for the spn equations, International Journal of Computer Mathematics 0 (0) (2019) 1–17. `arXiv:https://doi.org/10.1080/00207160.2019.1602768`, `doi:10.1080/00207160.2019.1602768`.
URL `https://doi.org/10.1080/00207160.2019.1602768`

[19] T. Takeda, H. Ikeda, 3-d neutron transport benchmarks, Journal of Nuclear Science and Technology 28 (7) (1991) 656–669.

[20] M. Capilla, C. Talavera, D. Ginestar, G. Verdú, Application of a nodal collocation approximation for the multidimensional pl equations to the 3d takeda benchmark problems, Annals of Nuclear Energy 40 (1) (2012) 1–13.